Practical approaches to seawater intrusion investigation and management

Leanne K. Morgan

B. App. Sc. (Hons), B. Sc., Grad. Dip. Ed.

Submitted in full for the degree of Doctor of Philosophy in the School of the Environment, Flinders University, South Australia

2014

Summary

Seawater intrusion (SWI) is the encroachment of saltwater into fresh coastal aquifers. It is a complex process that involves variable-density flow, solute transport and hydrochemical processes, which can make SWI assessment relatively difficult and expensive. The aim of this thesis is the development, application and critical assessment of practical (i.e., rapid, inexpensive) analytic modelling approaches for investigating and assisting in the management of SWI.

First, the steady-state, sharp-interface, analytic modelling approach of Werner et al. (2012) is applied to the Willunga Basin, South Australia in order to gain insight into the relative vulnerabilities of aquifers at the site. Vulnerability is assessed both for current conditions and future stresses (i.e., increased extraction, sea-level rise and recharge change). Limitations of the method, associated with the sharp-interface and steady-state assumptions, are addressed using numerical modelling to explore transient, dispersive SWI caused by sea-level rise. The study provides guidance for an ongoing field-based investigation of SWI.

Second, the Werner et al. (2012) approach is extended to the case of freshwater lenses on islands, accounting also for land surface inundation associated with sea-level rise. Equations are developed for both flux-controlled and head-controlled boundary conditions, which is consistent with the categorisation of continental coastal aquifers by Werner et al. (2012). The resulting equations provide general relationships between SWI vulnerability in freshwater lenses and hydrogeological conditions. Example applications to several case studies illustrate use of the method for rapidly ranking

lenses according to vulnerability, thereby allowing for prioritisation of areas where further and more detailed SWI investigations may be required.

The third study of this thesis considers the impact of SWI-induced changes in seawater volume on water-level trends (which are commonly used as a proxy for changes in aquifer storage), and coastal aquifer water balances. A steady-state, sharp-interface, analytic modelling approach was used to generate idealised relationships between seawater volume, freshwater volume and water levels. The approach assumes quasi-equilibrium conditions (i.e., steady-state conditions persist during temporal changes), which were evaluated using a selection of transient, dispersive simulations and found to be valid in the majority of cases. We conclude that changes in seawater volumes should be included routinely in coastal aquifer water balances. Also, temporal trends in coastal aquifer water levels may not provide an adequate measure of freshwater storage trends.

In the fourth study of this thesis, we investigate physical processes associated with transient seawater movement into coastal aquifers. Specifically, we use sand tank modelling to assess whether SWI overshoot is a measurable physical process. SWI overshoot has been recently reported within numerical modelling studies of transient sea-level rise and SWI by Watson et al. (2010) and Chang et al. (2011) and involves the freshwater-saltwater interface temporarily extending further inland than the eventual steady-state position. This implies that steady-state SWI may not be the worst case, as is generally assumed. In this study, sand tank modelling of sea-level rise and SWI was carried out and photographs show, for the first time, that an overshoot occurs under controlled laboratory conditions. A sea-level drop experiment was also carried out, and overshoot was again observed, whereby the interface was temporarily closer to the

coast than the eventual steady-state position. Numerical modelling corroborated the physical sea-level rise and sea-level drop experiments. This work demonstrates that commonly adopted steady-state approaches can under-estimate the maximum extent of SWI, due to the overshoot phenomenon.

Declaration

I certify that this thesis does not incorporate without acknowledgement any material previously submitted for a degree or diploma in any university; and that to the best of my knowledge and belief it does not contain any material previously published or written by another person except where due reference is made in the text.

Leanne K. Morgan

Acknowledgements

I wish to acknowledge the financial support of the Australian Research Council through the National Centre for Groundwater Research and Training (NCGRT). The work presented in this thesis would not have been possible without that support.

Thank you to my Principal Supervisor Adrian Werner for his enthusiasm, scientific guidance and editorial advice. Thank you also to my Co-Supervisors Vincent Post and Craig Simmons for their support and editorial comment. Thanks to Mark Bakker for hosting me at Delft University of Technology for 3 months during which time I gained many new insights into interface modelling. Thanks also to Jesus Carrera and Maria Pool (Technical University of Catalonia, Spain), Perry de Louw (Deltares, Netherlands), Leonard Stoeckl (Federal Institute for GeoSciences and Natural Resources, Germany), Eugenia Hirthe and Thomas Graf (Institute of Fluid Mechanics, Germany) for their generous hospitality, and for broadening my understandings of hydrogeology. I would also like to thank editors and reviewers of manuscripts presented in this thesis as well as the examiners of this thesis.

I also wish to acknowledge and thank the team at GeoSciences Australia, led by Baskaran Sundaram, with whom I worked on the National-Scale Vulnerability Assessment of Seawater Intrusion Project during my PhD.

It has been a great experience working with my NCGRT colleagues at Flinders University. Thanks to Daan and Chani for making our office a nice place to be.

And thank you to my family and friends, especially Keith, for their care and patience.

Table of Contents

List of Figures

List of Tables

Chapter 1

Introduction

1.1 Objectives

Coastal aquifers are major sources of freshwater supply in many countries (Cheng et al., 2004). Under natural, undisturbed conditions, a landward hydraulic gradient exists within coastal aquifers, with freshwater discharging to the sea. A wedge of saltwater extends beneath the freshwater, due to density differences. Changes in the hydrology of the coastal zone can cause landward movement of seawater, a process referred to as seawater intrusion (SWI). SWI causes degradation of groundwater quality through the displacement of fresh groundwater by seawater.

There is increased risk of SWI in the future due to sea-level rise (SLR), climate change and the increasing dependence on coastal fresh groundwater resources for water supply (Barlow and Reichard, 2010; Post, 2005; Werner, 2010; Werner et al., 2013). Some coastal aquifers, such as freshwater lenses of small islands, are especially vulnerable to SWI caused by the aforementioned factors (White and Falkland, 2010). Understanding SWI is therefore very important if coastal freshwater resources are to be managed sustainably.

SWI is a complex process and this makes SWI assessment relatively difficult and expensive (Werner et al., 2013). While management of coastal aquifers will ideally involve field-based investigations and the development of complex numerical models,

management decision-making often requires rapid assessments of coastal aquifer vulnerability to SWI. In some instances, a simplified approach may be all that is affordable, for example in the case of large-scale (i.e., national or continental) studies. In such cases, first-order assessment methods involving analytic interface modelling are a practical choice and can be used to identify areas where further, more detailed SWI assessment may be required. Analytic modelling is also a reasonable choice when reliable input data for a sophisticated model are not available. The usefulness of analytic models as instructional tools for providing insights into the mechanical trend of the flow and steady-state interface location has been advocated by many researchers (Bear, 1972; Strack, 1989; Haitjema, 1995; Cheng, 1999; Custodio, 1987).

Analytic interface models, as described by Strack (1976, 1989), simplify the SWI problem by: (1) neglecting mixing processes (i.e., assuming a sharp interface between the freshwater and saltwater); (2) assuming the saltwater to be stagnant; (3) adopting the Dupuit approximation (i.e., neglecting vertical resistance to flow); (4) adopting steady-state conditions. The steady-state interface position can then be estimated using the Ghyben-Herzberg relation (Ghyben, 1888; Herzberg, 1901). The Strack (1976, 1989) single-potential approach differs to others presented within the literature (e.g., Custodio, 1987) because it allows for a mathematically unified solution to a problem where the domain extends beyond the edge of the interface. As such, the Strack (1976, 1989) approach is well suited to regional-scale SWI modelling.

Recently, the analytic sharp-interface equations of Strack (1976) were used by Werner et al. (2012) as the basis for developing SWI vulnerability indicators for a range of conditions. The Werner et al. (2012) method is an improvement on existing large-scale

SWI vulnerability assessment approaches, such as GALDIT (Lobo-Ferreira et al., 2007) and CVI(SLR) (Ozyurt, 2007), because it is theoretically based and therefore incorporates the physical mechanics of SWI, albeit under highly idealised conditions. The basic premise is that partial derivative equations quantify the propensity for SWI, as rates of change in SWI extent, for a range of different stresses (e.g., increased extraction, reduced recharge and SLR). Using this approach, SWI vulnerability (defined as the propensity for SWI to occur) can be easily and rapidly quantified.

This thesis starts (Chapter 2) with a description of the practical application of the Werner et al. (2012) approach within a first-order assessment of SWI vulnerability for the Willunga Basin aquifer system in South Australia. The objective here is to obtain insight into the relative vulnerabilities of the Willunga Basin aquifers, which will assist in the determination of research priorities as part of an on-going field-based investigation of the Willunga Basin. Limitations of the vulnerability indicators method, associated with the sharp-interface and steady-state assumptions, are addressed using numerical modelling to explore transient, dispersive SWI caused by SLR. The SWI vulnerability indicators have subsequently been applied (using the approach described in this chapter) to 28 case study areas as part of a national-scale assessment of SWI vulnerability for Australia, as described in Ivkovic (2012), Morgan et al. (2013b) and Morgan et al. (2013c).

Despite widespread concern regarding the vulnerability of freshwater lenses to SWI (e.g., Chui and Terry, 2013; Church et al., 2006; Mimura, 1999; Terry and Chui, 2012; White et al., 2007; White and Falkland, 2010; Woodroffe, 2008), there is currently little guidance on methods for rapidly assessing the vulnerability of freshwater lenses to the

potential effects of climate change. The second objective of this thesis (Chapter 3) is to extend the Werner et al. (2012) vulnerability indicators methodology to freshwater lenses in strip islands. Given the high susceptibility of many low-lying oceanic islands to land surface inundation (LSI) by the ocean (White and Falkland, 2010), the influence of LSI on SWI vulnerability is also considered.

The primary focus of coastal aquifer management studies is most commonly the inland movement of saltwater and associated threats to water supplies (e.g., Mantoglou, 2003; Werner and Gallagher, 2006). The loss of freshwater storage arising from SWI has received considerably less attention. In many cases, the volumes of storage loss caused by SWI are neglected in evaluating coastal aquifer water balances, despite the importance of accurate quantification of water budgets for management purposes (Bredehoeft, 2002; Custodio, 2002). The estimation of SWI-induced storage decline in practice is confounded by difficulties in quantifying interface movements, which are often poorly constrained because salinity measurements are usually sparse and infrequent. Hence, freshwater storage losses from interface movements are often undetected and subsequently not accounted for. The third objective (Chapter 4) is to examine the conditions under which this may be a significant oversight in the assessment of coastal aquifer condition, i.e., where hydrograph trends are adopted as an indicator of storage depletion (e.g., Brown, 2006; Bekesi, 2009) and freshwater-only water balances are used to develop management strategies (e.g., Davidson and Yu, 2006; Schafer and Johnson, 2009; Sun, 2005; Varma, 2009; Voudouris, 2006; Zulfic et al., 2007). A steady-state, sharp-interface, analytic modelling approach is used to generate idealised relationships between seawater volume, freshwater volume and water

levels. The approach assumes quasi-equilibrium conditions, which are evaluated using a selection of transient, dispersive simulations.

In recent years, a number of numerical modelling studies (e.g., Chang et al., 2011; Watson et al., 2010) of transient SLR-SWI have reported an overshoot phenomenon, whereby the freshwater-saltwater interface temporarily extends further inland than the eventual steady-state position. SWI overshoot may have significant implications for coastal aquifer management, because it implies that the post-SLR steady-state interface position may not be the worst case, as is generally assumed. The final objective (Chapter 5) of this thesis is to use physical and numerical modelling to address the question of whether SWI overshoot is a measurable physical process, or simple a nuance of numerical modelling.

The following four Chapters are taken directly from a book chapter (Chapter 2) and international journal publications (Chapters 3, 4, 5). Each Chapter can therefore be read independently. The reference for the book chapter and papers is provided as a footnote at the start of each Chapter. Chapter 6 summarises the main results and conclusions of this thesis.

Chapter 2

Application of a rapid-assessment method for seawater intrusion vulnerability: Willunga Basin, South Australia

Abstract

SWI causes degradation of water quality and loss of water security in coastal aquifers. Although the threat of SWI has been reported in all of the Australian states and the Northern Territory, comprehensive investigations of SWI are relatively uncommon because SWI is a complex process that can be difficult and expensive to characterise. The current study involves the application of a first-order method developed recently by Werner et al. (2012) for rapidly assessing SWI vulnerability. The method improves on previous approaches for the rapid assessment of large-scale SWI vulnerability, because it is theoretically based and requires limited data, although it has not been widely applied. In this study, the Werner et al. (2012) method is applied to the Willunga Basin,

---

This Chapter is based on the following publication: Morgan LK, Werner AD, Morris MJ, Teubner MD, 2013. Application of a rapid-assessment method of SWI: Willunga Basin, South Australia, In: Wetzelhuetter, C. (Ed.), Groundwater in the Coastal Zones of Asia - Pacific, Coastal Research Library, Vol. 7, Springer.

South Australia to explore SWI vulnerability arising from extraction, recharge change and sea-level rise (SLR). The Willunga Basin is a multi-aquifer system comprising the unconfined Quaternary (Qa) aquifer, confined Port Willunga Formation (PWF) aquifer and confined Maslin Sands (MS) aquifer. Groundwater is extracted from the PWF and MS aquifers for irrigated agriculture. In the Qa aquifer, the extent of SWI under current conditions was found to be small and SWI vulnerability, in general, was relatively low. For the PWF aquifer, SWI extent was found to be large and SWI is likely to be active due to change in heads since pre-development. Anecdotal evidence from recent drilling in the PWF aquifer suggests a seawater wedge that extends at least 2 km from the coast. A relatively high vulnerability to future stresses was determined for the PWF aquifer, with key SWI drivers being SLR (under head-controlled conditions, which occur when aquifer heads are fixed within an aquifer due to, for example, pumping) and changes in flows at the inland boundary (as might occur if extraction increases). The MS aquifer was found to be highly vulnerable because it has unstable interface conditions whereby the interface is moving inland and a steady-state condition cannot be calculated.. Limitations of the vulnerability indicators method, associated with the sharp-interface and steady-state assumptions, are addressed using numerical modelling to explore transient, dispersive SWI caused by SLR of 0.88 m. Both instantaneous and gradual (linear rise over 90 years) SLR impacts are evaluated for the Qa and PWF aquifers. A maximum change in wedge toe of 50 m occurred within 40 years (for instantaneous SLR) and 100 years (for gradual SLR) in the Qa aquifer. In the PWF aquifer, movement of the wedge toe was about 410 m and 230 m after 100 years, for instantaneous and gradual SLR, respectively. Steady state had not been reached after 450 years in the PWF aquifer. Analysis of SLR in the MS aquifer was not possible due to unstable interface conditions. In general, results of this study highlight the need for further

detailed investigation of SWI in the PWF and MS aquifers. Establishing the extent of SWI under current conditions is the main priority for both the PWF and MS aquifers. An important element of this involves research into the offshore extent of these aquifers. Further, predictions of SWI in the PWF aquifer should consider future extraction and SLR scenarios in the first instance. A field-based investigation of the Willunga aquifer is ongoing, and the current study provides guidance for well installation and for future data collection.

2.1 Introduction

In coastal aquifers, changes in the hydrology of the coastal zone can cause landward movement of seawater (i.e., saline groundwater), a process referred to as seawater intrusion (SWI). Historically, the occurrence of SWI has been linked to excessive groundwater pumping or groundwater discharge to surface features, and these have led to significant losses in the available freshwater resources in coastal aquifers worldwide (FAO, 1997). However, climate change impacts (e.g., sea-level rise (SLR) and reductions in aquifer recharge) can also induce SWI (e.g., Post, 2005). Therefore, the vulnerability of coastal aquifers to climate change, increased levels of extraction and SLR should be jointly considered in water management investigations.

In Australia, where over 85% of the population live within 50 km of the coast (ABS, 2004), SWI poses a threat to groundwater resources in all of the states and the Northern Territory (Werner et al., 2010). However, the extent of monitoring and investigations specific to SWI are highly variable across the nation, with detailed SWI investigations having occurred in only a few areas (Werner et al., 2010). A method for rapid first-

order assessment of SWI vulnerability is needed to identify current and emerging risk areas, along with the key drivers of SWI in these areas. This information can then be used to prioritise areas requiring more detailed SWI investigations in the future.

SWI is a complex process that involves variable-density flow, solute transport and hydrochemical processes (Werner et al., 2013), which can make SWI assessment relatively difficult and expensive. As a result, the assessment of SWI vulnerability over large scales has been carried out using mainly qualitative methods, such as GALDIT (Lobo-Ferreira et al. 2007) and CVI(SLR) (Ozyurt, 2007), which consider only a subset of the factors thought to impact SWI. For example, aquifer fluxes are not accounted for, and SWI vulnerability arising from changes in sea-level, recharge or extraction, are not captured directly, if at all. Also, these methods largely lack a theoretical basis and rather they focus subjectively on a selection of the elements associated with SWI.

Recently, an alternative to the above-mentioned large-scale methods has been developed by Werner et al. (2012). The method is based on the steady-state, sharp-interface equations of Strack (1976), and therefore incorporates the physical mechanics of SWI, albeit under highly idealised conditions. Werner et al. (2012) described the development of a range of simple SWI vulnerability indicator equations for unconfined and confined aquifer systems. The basic premise is that partial derivative equations quantify the propensity for SWI as rates of change in SWI extent for a range of different stresses (e.g., increased extraction, reduced recharge and SLR). Using this approach, SWI vulnerability (defined as the propensity for SWI to occur) can be easily and rapidly quantified. A relatively small number of hydrogeological parameters are required for the method, making it suitable for application within data poor areas. Further, SWI

vulnerability to different stresses can be readily compared using this approach, given the simple nature of the underlying equations. Werner et al. (2012) applied the method to a number of coastal aquifer systems, where detailed SWI assessments have been carried out, and found a general agreement between their approach and the vulnerability determinations obtained from more detailed investigations.

The steady-state analysis of Werner et al. (2012) does not provide information on SWI transience (i.e., variability with time); despite that the method is considered an improvement over previous large-scale approaches. Nevertheless, failure to account for SWI transience is arguably a significant limitation, given that the perceived importance of any water resource issue is likely to be a combination of both the magnitude and the immediacy of the event. The lack of temporal insights is a common short-coming of analytical SWI methods (Cheng and Ouazar, 1999). Exploration of SWI transience generally necessitates the use of variable-density flow and transport numerical models, which involve a greater degree of complexity and computational effort than analytical approaches. Hence, it is commonplace to undertake cross-sectional 2D numerical modelling to limit the computational effort of transient, dispersive modelling. Watson et al. (2010) and Webb and Howard (2011) used 2D numerical simulations to show that SWI time scales (i.e., the time for new steady-state conditions to be reached following a SLR event) is typically in the order of decades to centuries, at least for idealised hydrogeological conditions. Watson et al. (2010) found that in some cases, an over-shoot in the seawater wedge occurred whereby the final steady-state location was temporarily exceeded during transient simulations, suggesting that steady-state may not be the worst case, as had previously been thought. These findings highlight the importance of exploring SWI transience as a next step following steady-state SWI

assessment (or other first-order analyses), even if a relatively simple and idealised aquifer conceptualisation is used for transient analysis.

In this study, we apply the recently developed method of Werner et al. (2012) for the rapid assessment of SWI that is suitable for use when limited data are available and large areas are to be considered. The method is applied to the Willunga Basin, South Australia, which was selected because it is typical of many Australian coastal aquifer systems at risk of SWI, in that there are currently no SWI-specific monitoring, modelling or management in place. In addition, the Willunga Basin is a multiple aquifer system and, as such, allows demonstration of the method for both unconfined and confined aquifer systems. As an extension to the Werner et al. (2012) method, we examine transient effects, by evaluating the temporal development of SWI under conditions similar to those of the Willunga Basin, as induced by projected SLR.

2.2 Theory

2.2.1 Analytical approach

The analytic solution for the steady-state location of the freshwater-seawater interface developed by Strack (1976, 1989) is the basis for the method described by Werner et al. (2012), and summarised here. Figure 1 illustrates the conceptual model for unconfined and confined aquifers.

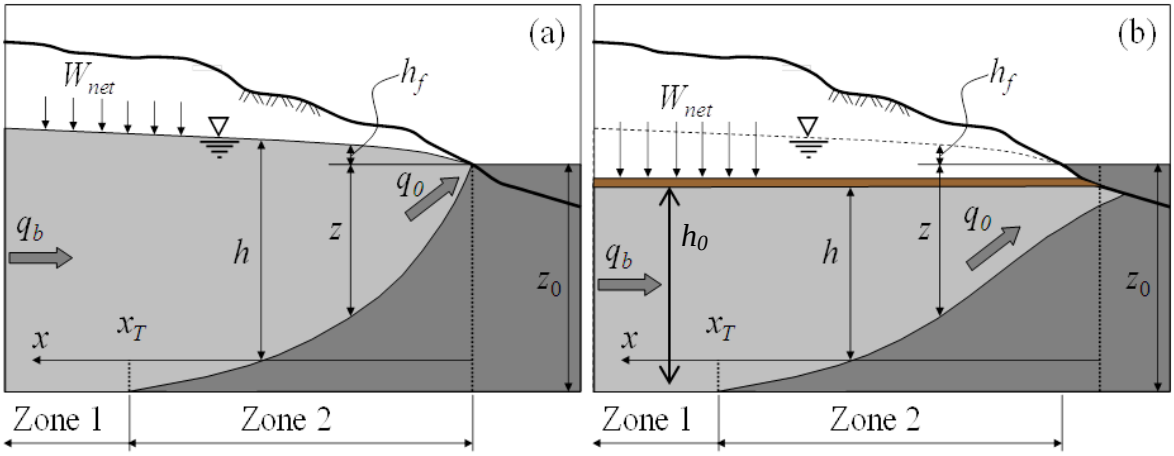

Figure 1. Description of hydrogeological variables for: (a) unconfined aquifer and (b) confined aquifer settings (adapted from Werner et al., 2012)

The water budget for the problem domain, as shown in Figure 1, is comprised of net recharge (W_{net} [L/T], accounting for infiltration, evapotranspiration and distributed pumping), freshwater discharge to the sea (q_0 [L^2/T]), and lateral flow from aquifers inland of the landward boundary (q_b [L^2/T]). The hydraulic head (h_f [L]) is related to the depth of the interface (z [L]) by the Ghyben-Herzberg relation: $z = h_f / \delta$. Here, δ [-] is the dimensionless density ratio $\delta = (\rho_s - \rho_f)/\rho_f$, and ρ_s (= 1025 kg/m^3) and ρ_f (= 1000 kg/m^3) are freshwater and seawater densities, respectively [M/L^3], so that δ = 0.025. The freshwater thickness is h [L], and the base of the aquifer is z_0 [L] below mean sea level. In the confined aquifer, the saturated aquifer thickness in Zone 1 is h_0. Zone 1 is the region inland of the saltwater wedge and Zone 2 is the region between the coast and the inland extent (x_T) of the saltwater wedge. From a conceptual perspective, while the problem domain is theoretically infinite in the landward direction, the cross section is assumed to occur in a coastal fringe of between 1 km and 5 km from the coast.

2.2.1.1 Unconfined aquifers

Strack (1976) used the potential method to produce equations for h_f as a function of aquifer parameters and distance from the coast x [L]. In Zone 1 ($x \geq x_T$; Figure 1a):

$$h_f = \sqrt{\frac{2q_0 x - W_{net} x^2}{K} + (1 + \delta) z_0^2} - z_0 \quad (1)$$

In Zone 2 ($x \leq x_T$; Figure 1a):

$$h_f = \sqrt{\left(\frac{\delta}{1+\delta}\right)\frac{2q_0 x - W_{net} x^2}{K}} \quad (2)$$

Here, K is the hydraulic conductivity [L/T] and other parameters are defined above. Equations (1) and (2) can be rearranged to allow for the estimation of q_0 for a given h_b at x_b from the coast (i.e., obtained from monitoring well observations), and using estimates of the other aquifer parameters (K, z_0, δ, W_{net}). In Zone 1:

$$q_0 = \frac{K\left((h_b + z_0)^2 - (1+\delta) z_0^2\right) + W_{net} x_b^{\,2}}{2x_b} \quad (3)$$

In Zone 2:

$$q_0 = \left(\frac{1+\delta}{\delta}\right)\frac{K}{2x_b} h_b^2 + \frac{W_{net} x_b}{2} \quad (4)$$

Note that the choice of equations (3) or (4) for estimating q_0 depends on whether the given h_b value occurs within Zone 1 (i.e., head measurement is inland of the interface) or Zone 2 (i.e. head measurement is above the interface). The location of the wedge toe x_T [L] (see Figure 1) is derived through considering that $h_f = \delta z_0$ at the wedge toe. In

situations where recharge (e.g. from rainfall) exceeds the combined outflows from distributed pumping and groundwater evapotranspiration (i.e., $W_{net} > 0$), the wedge toe is obtained from (Cheng and Ouazar, 1999):

$$x_T = \frac{q_0}{W_{net}} - \sqrt{\left(\frac{q_0}{W_{net}}\right)^2 - \frac{K\delta(1+\delta)z_0^2}{W_{net}}} \quad (5)$$

The conceptualisation of Figure 1a assumes that a no-flow boundary occurs at some inland distance. That is, the lateral inflow is zero ($q_b = 0$) at some distance (x_n) from the coast. By considering the water balance, the value of x_n is given as (Werner et al., 2012):

$$x_n = q_0 / W_{net} \quad (6)$$

As the wedge toe approaches x_n, there is progressively less freshwater discharge to oppose the inland movement of the seawater wedge. In other words, the distance x_n serves as a practical limit to the extent of SWI in the aquifer. Conditions causing the wedge toe to reach or exceed x_n (i.e., $x_T \geq x_n$) are more likely to be associated with adverse SWI events.

One of the advantages of using analytical equations in assessing problems such as SWI vulnerability is that parameter combinations are identifiable from the relevant equations. For example, equation (5) can be written in a simplified form, as (Werner et al., 2012):

$$x_T = x_n\left(1 - \sqrt{1 - M}\right) \quad (7)$$

Here, M [-] is a useful dimensionless combination of parameters that can be directly related to the SWI conditions, and is defined as (Werner et al., 2012):

$$M = \frac{K\delta(1+\delta)z_0^2}{W_{net}x_n^2} \tag{8}$$

Werner et al. (2012) termed M a "mixed convection ratio", because the numerator describes the density-driven processes causing landward migration of the wedge, whilst the denominator represents freshwater advection processes that oppose SWI. If $M \geq 1$, the density-driven processes dominate, creating an unstable SWI situation (i.e., high SWI vulnerability). As such, M is a useful SWI vulnerability measure.

Seawater volume is adopted in this study as an alternative to x_T for quantifying the extent of SWI. The volume of seawater V_{sw} [L^3/L] per metre of coastline is found from the area (in cross section perpendicular to the shoreline) of the saltwater wedge, which is determined by integrating the interface equation (i.e., obtained by combining equation (2) and the relationship $z = h_f/\delta$) between the coast ($x = 0$) and the toe ($x = x_T$). For the case $W_{net} > 0$, the following equation is derived (Werner et al., 2012):

$$V_{sw} = n\, z_0 \left(x_T - \frac{x_n}{2} \left(\sqrt{\frac{1}{M}}\, \arcsin\left(\sqrt{M}\right) - \sqrt{1-M} \right) \right) \tag{9}$$

Here, n is porosity [-].

2.2.1.2 Confined aquifers

As with unconfined aquifers, Strack (1976) used the potential method to produce equations for h_f as a function of aquifer parameters and with distance from the coast in confined aquifers. In Zone 1 ($x \geq x_T$; Figure 1b):

$$h_f = \frac{q_0 x - W_{net}\dfrac{x^2}{2}}{Kh_0} + \delta z_0 - \frac{\delta h_0}{2} \tag{10}$$

In Zone 2 ($x \le x_T$; Figure 1b):

$$h_f = \sqrt{\left(2q_0 x - W_{net} x^2\right)\frac{\delta}{K}} + \delta z_0 - \delta h_0 \tag{11}$$

Parameters used here have been defined previously. Equations (10) and (11) can be re-arranged to allow for the estimation of q_0 from a given h_b (i.e., obtained from monitoring well observations) at x_b from the coast. In Zone 1:

$$q_0 = \frac{K}{2\delta x_b}\left(2\delta h_b h_0 + \left(\delta h_0\right)^2 - 2\delta^2 z_0 h_0\right) + \frac{W_{net} x_b}{2} \tag{12}$$

In Zone 2:

$$q_0 = \frac{K}{2\delta\, x_b}\left(h_b + \delta h_0 - \delta z_0\right)^2 + \frac{W_{net} x_b}{2} \tag{13}$$

The choice of equations (12) or (13) for estimating q_0 depends on whether the given h_b value occurs within Zone 1 or Zone 2, as previously. x_T can again be derived by considering that $h_f = \delta z_0$ at the wedge toe. We adopt cases where W_{net} = 0, because recharge to the Willunga Basin confined aquifers is poorly constrained and likely to be small within the coastal zone given the lithology, and also this is a common first-order assumption (e.g., Custodio, 1987). This leads to (Werner et al., 2012):

$$x_T = \frac{\delta K h_0^2}{2q_0} \tag{14}$$

The volume of seawater (per metre of coastline) is found from the area of the saltwater wedge, obtained through integrating the interface equation between $x = 0$ and $x = x_T$, to produce (Werner et al., 2012):

$$V_{sw} = \frac{n\delta K h_0^{\,3}}{6q_0} \tag{15}$$

The confined aquifer conceptualisation used here does not account for continuation of aquifers off-shore and may therefore result in overestimation of the landward position of the interface in confined aquifers. Analytic solutions presented by Bakker (2006) and Kooi and Groen (2001) account for offshore continuation of confined aquifers. However, information on parameters required for the method (e.g., distance the aquifer extends off-shore and the vertical hydraulic conductivity of the semi-confining aquitard) are not available for the Willunga Basin aquifers. Therefore, the approach adopted here assumes that freshwater discharges from the confined aquifer at the coastline, in line with the Werner et al. (2012) approach.

The density-corrected freshwater head in a confined aquifer terminating at the coast is:

$$h_{coast} = \delta(z_0 - h_0) \tag{16}$$

Equation (16) is derived from equation (11) when $x = 0$. The freshwater head in the aquifer and close to the coast (e.g., from observation wells) needs to be greater than this value for there to be freshwater discharge (i.e., $q_0 > 0$) and to avoid active SWI, i.e., SWI occurring under a hydraulic gradient causing inland flow. It is important to compare aquifer heads with the density-corrected head at the coast (obtained from equation (16)) because equation (13) provides a positive q_0 value (due to the squared

bracketed term) even when the head in the aquifer is less than the head at the coast (i.e., when $h_b < h_{coast}$), and this can lead to erroneous results for q_0, x_T and V_{sw}. If the aquifer continues offshore, the head required for freshwater discharge will be greater than that described by equation (16).

2.2.1.3 SWI Vulnerability indicators

The sensitivity of SWI to different stresses has been characterised by Werner et al. (2012) using partial derivative equations. These equations describe the propensity for the wedge toe to change with changes in sea level, recharge or inflows at the inland boundary (as might occur due to increased extraction). Werner and Simmons (2009) found that the impact of SLR in unconfined coastal aquifers is greater in head-controlled systems (where groundwater abstractions or surface water features maintain the head in the aquifer despite SLR) than in flux-controlled systems (where groundwater discharge to the sea remains constant despite SLR). In line with these findings, Werner et al. (2012) developed derivative equations relating to both head-controlled and flux-controlled systems. A number of the derivative equations, which will be applied to the Willunga Basin case study, are presented in Table 1. Derivatives associated with changes in recharge are not presented for the confined aquifers because, as previously mentioned, an assumption of zero net recharge has been made for the Willunga Basin confined aquifers. Werner et al. (2012) provides further details, including assumptions applied in deriving these equations.

Table 1. SWI Vulnerability indicator equations (adapted from Werner et al., 2012)

<table>
<tr><th colspan="2">Unconfined aquifers</th></tr>
<tr><td>Flux-controlled setting</td><td>Head-controlled setting</td></tr>
<tr><td>SLR
$\frac{\partial x_T}{\partial z_0} = \frac{x_n M}{z_0\sqrt{1-M}}$ (17)</td><td>SLR
$\frac{\partial x_T}{\partial z_0} = \frac{x_n M}{z_0\sqrt{1-M}} + \frac{x_n M}{\delta z_0}\left(\frac{1-\sqrt{1-M}}{\sqrt{1-M}}\right)$ (18)</td></tr>
<tr><td>Change in net recharge
$\frac{\partial x_T}{\partial W_{net}} = -\frac{x_n M}{2W_{net}\sqrt{1-M}}$ (19)</td><td>Change in net recharge
$\frac{\partial x_T}{\partial W_{net}} = -\frac{x_n M}{2W_{net}\sqrt{1-M}} + \frac{x_n\left(1-\sqrt{1-M}\right)}{2W_{net}\sqrt{1-M}}$ (20)</td></tr>
<tr><td colspan="2">Change in flux at the inland boundary
$\frac{\partial x_T}{\partial q_b} = \frac{1}{W_{net}}\left(1-\frac{1}{\sqrt{1-M}}\right)$ (21)</td></tr>
<tr><th colspan="2">Confined aquifers</th></tr>
<tr><td>Flux-controlled setting</td><td>Head-controlled setting</td></tr>
<tr><td>SLR, where $W_{net} = 0$
$\frac{\partial x_T}{\partial z_0} = 0$ (22)</td><td>SLR, where $W_{net} = 0$
$\frac{\partial x_T}{\partial z_0} = \frac{\delta(1+\delta)K^2 h_0^3}{2q_0^2 x_f}$ (23)</td></tr>
<tr><td colspan="2">Changes in inflows at the inland boundary, where $W_{net} = 0$
$\frac{\partial x_T}{\partial q_b} = \frac{\partial x_T}{\partial q_0} = -\frac{\delta K h_0^2}{2q_0^2}$ (24)</td></tr>
</table>

2.2.2 Transient analysis

The transience of SWI arising from SLR was explored using a selection of 2D simulations. The variable-density flow and solute transport code SEAWAT (Version 4; Langevin et al., 2008) was used. Description of the numerical methods and equations used in SEAWAT are given by Guo and Langevin (2002) and Langevin et al. (2008).

2.3 Application to the Willunga Basin

2.3.1 Conceptualisation and parameterisation of the Willunga Basin

The Willunga Basin is situated south of Adelaide in South Australia, as shown in Figure 2. The Willunga Basin is an important food-production region and groundwater is used to irrigate for the production of almonds, grapes and olives. The four main aquifers within the Willunga Basin are the unconfined Quaternary aquifer (Qa) (comprised of sands, gravels and interbedded clays), the confined Port Willunga Formation aquifer (PWF) (loosely consolidated sands and indurated limestone), the confined Maslin Sands aquifer (MS) (very fine to coarse sands) and a fractured basement rock aquifer (FR). The majority of salinities are less than 1500 mg/L in all four of these aquifers and groundwater is generally considered suitable for irrigation purposes, despite some individual monitoring locations recording significantly higher salinities (Obswell network, https://obswell.pir.sa.gov.au/).

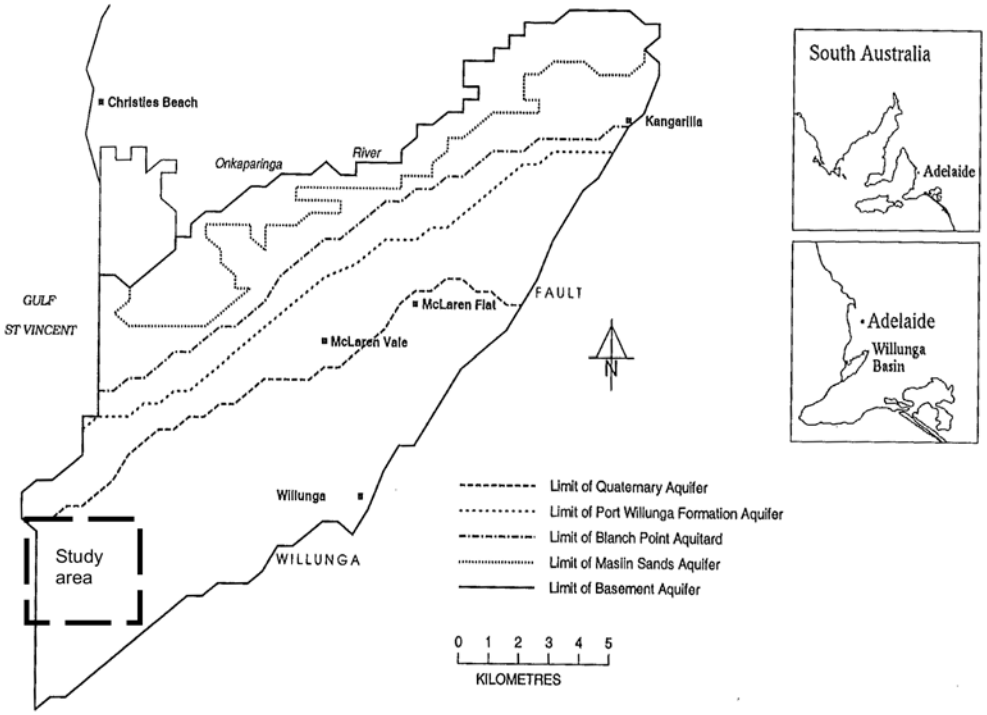

Figure 2. The Willunga Basin location and extent of hydrogeological units (based on Rasser, 2001)

The majority of the metered groundwater extraction is from the PWF aquifer, followed by the MS and FR aquifers. Although groundwater use is regulated under state water allocation planning frameworks, the existing coastal groundwater network is not appropriate for monitoring potential SWI impacts, because observation wells do not penetrate to the base of the aquifers (where any SWI would most likely be observed). However, anecdotal evidence from recent drilling conducted within the Basin's coastal fringe suggests salinity impacts in wells drilled to near the base of the PWF aquifer. Field-measured electrical conductivity (EC) during air lifting of two pilot trial aquifer storage and recovery injection wells located at 1300 m and 1800 m from the coast indicated EC values of around 20 mS/cm (~12,000 mg/L) and 40 mS/cm (~24,000 mg/L), respectively, well outside the average aquifer salinity of 1500 mg/L. Salinity impacts were not observed during development of two adjacent, shallower wells

constructed within the PWF implying a seawater wedge configuration, consistent with SWI and a seawater wedge that is at least 2 km from the coast in the PWF.

The study area selected for the analysis is identified in Figures 2 and 3. It covers a distance of approximately 3500 m of coastline and has an inland boundary approximately 3500 m from the coast. The aquifers included in the assessment are the Qa, PWF and MS sequences. The FR aquifer was not considered due to lack of water level and aquifer geometry data.

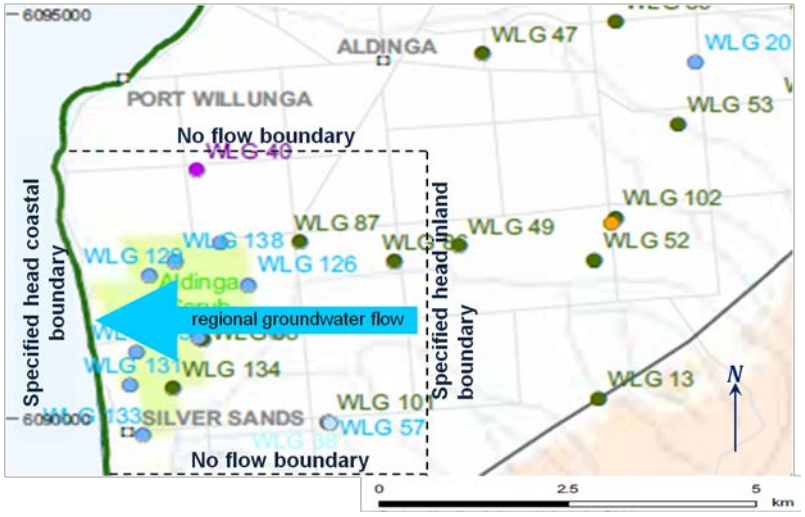

Figure 3. Study area for Willunga Basin conceptualisation, with towns (e.g., Port Willunga) and monitoring boreholes (e.g., WLG47) identified

The Willunga Basin parameters required for the Werner et al. (2012) equations were obtained from the following sources: site-specific reports (for net recharge values; Herczeg and Leaney (2002)); review of hydrographs using the Obswell network (for heads in the different aquifers); interpretation of lithological logs from the Drillhole Enquiry System (https://des.pir.sa.gov.au/deshome.html) and Obswell (for aquifer geometry); and application of literature values (for hydraulic conductivity and porosity) typical of the study area lithologies. Pump test information was not available for the

coastal region of the Willunga Basin. The resulting parameter values are shown in Table 2. In estimating W_{net}, it was assumed that all extraction occurs inland of the 3500 m inland boundary. As such, W_{net} represents rainfall recharge for the Qa aquifer, and W_{net} is zero for the PWF and MS aquifers, as previously mentioned. An estimated pre-development (i.e., pre-pumping) head was also needed for the analysis of the PWF aquifer, and this was based on historical maximum heads.

Table 2. Hydrogeological parameters for the Willunga Basin aquifers

Aquifer	K (m/d)	W_{net} (mm/yr)	z_0 (m)	h_0 (m)	h_b (m)	x_b (m)	n (-)
Qa (Unconfined)	10	20	20	-	3.0	3500	0.3
PWF (Confined)	10	0	120	90	1.5 (3.0)*	3500	0.3
MS (Confined)	1	0	225	65	2.0	3500	0.3

*Estimated pre-development head.

2.3.2 Theoretical SWI extent in the Willunga Basin

The hydrogeological parameters listed in Table 2, along with equations (3), (5), (8), (9), (13), (14) and (15) were used to estimate discharge to the sea and the theoretical steady-state extent of SWI within each aquifer, as shown in Table 3. These results represent the theoretical long-term (i.e., steady-state) condition of the system based on modern-day stresses, unless otherwise stated.

Table 3. Results indicating theoretical SWI extent for the Willunga Basin aquifers

Aquifer	q_0 (m^2/d)	q_0 equation	x_T (m)	M (-)	V_{sw} (m^3/m)
Qa (Unconfined)	0.27	(3)	197	0.08	390
PWF (Confined)	0.03 (0.29)*	(13)	31500 (3500)*	NA	283500 (31500)*
MS (Confined)	<0.00	(13)	Unstable	NA	Unstable

*Calculated pre-development values.

The estimated inland extent of SWI in the Qa aquifer is relatively small, and the low M value suggests that SWI vulnerability is also low. For the PWF aquifer, the theoretical inland distance to the toe is very large (>31 km) under current conditions. This value exceeds the inland limit of the coastal fringe (x_b = 3500 m) and is indicative of an extensive seawater wedge. The q_0 calculated using pre-development conditions is almost 10 times the value under current conditions. The difference between the current and pre-development values of V_{sw} indicates that a large volume of seawater has entered (or will eventually enter) the PWF since the pre-development period.

The confined MS aquifer was found to have a hydraulic gradient that sloped downwards toward the inland (the head at the coast, calculated using equation (16), was 4.0 m AHD, while the head in the aquifer was estimated at 2.0 m AHD). This implies that the value of q_0 is negative (no freshwater discharge to the sea, but rather seawater flows inland), which suggests unstable interface conditions. Under these circumstances, the wedge toe is probably moving inland (notwithstanding the limitations of the steady-state analysis and the likely off-shore extension of the confined aquifer), creating the most extensive SWI over long timeframes. It is not possible to calculate x_T or V_{sw} for the MS aquifer due to the theoretically unstable interface condition. However, the

location of the interface stability limit (i.e., for h_b = 4.0 m AHD) is shown in Figure 4, along with the steady-state interface for the unconfined Qa and confined PWF within the coastal fringe. Given the approximate nature of the analysis, the interface and water table distributions shown in Figure 4 are not intended as accurate representations for the Qa, PWF and MS aquifers. Rather, the results provide a rough guide to the likely steady-state extent of seawater in the aquifer, under current-day stresses. In the case that the PWF aquifer (and the MS aquifer) extend significant distances off-shore, the results presented here will tend to over-estimate the inland extent of the interface in these aquifers.

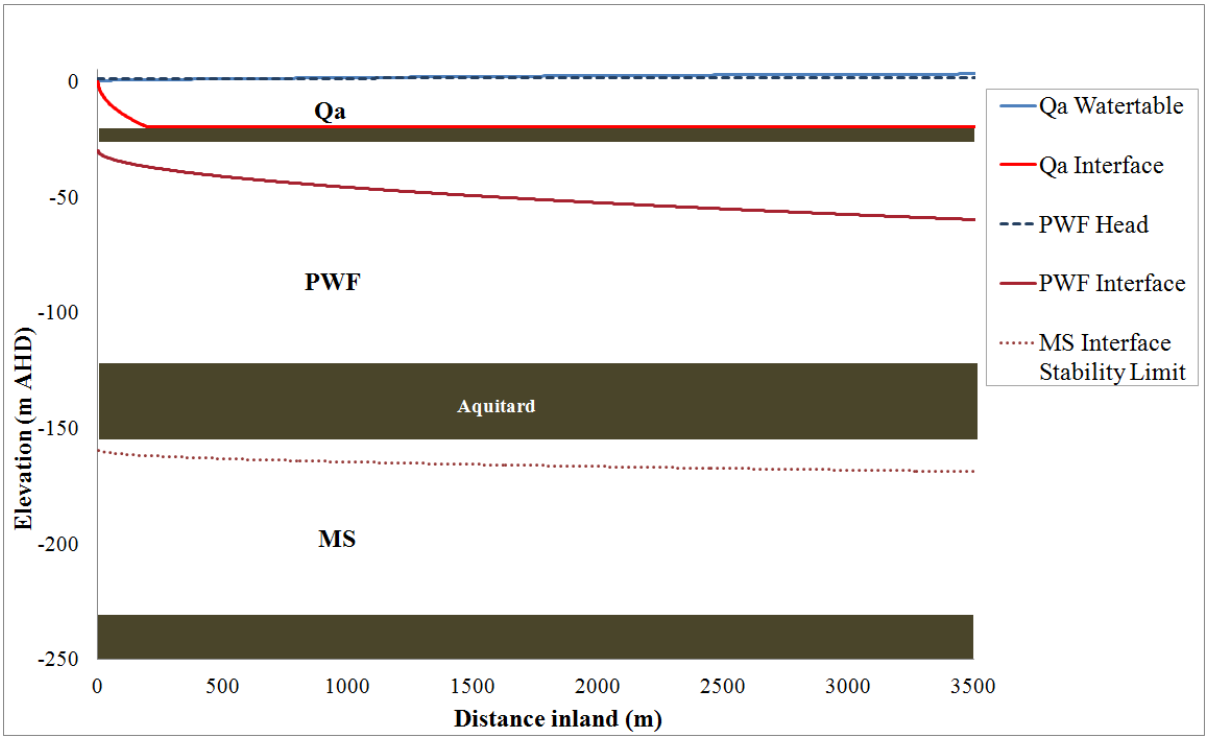

Figure 4. Approximation of the near-coastal water table and interface locations for the Willunga Basin aquifers

2.3.3 SWI vulnerability indicators for the Willunga Basin

SWI vulnerability indicators were calculated using equations (17) to (24) and parameters in Table 2 for the Qa and PWF aquifers. Vulnerability indicators could not be calculated for the MS aquifer as it is theoretically unstable; however, it can be inferred that the already high potential vulnerability of the MS aquifer will increase under increased stresses associated with climate change and pumping. Werner et al. (2012) began a database of aquifers for which SWI vulnerability indicators were calculated and these are presented in Table 4, along with results for the Willunga Basin analysis. The addition of more cases to this database allows for an improved relative assessment of SWI vulnerability. In Table 4, Cases 1a to 1c represent three scenarios associated with the Gaza unconfined aquifer investigation by Moe et al. (2001); specifically 1a represents undisturbed conditions, 1b represents full implementation of a management plan, and 1c is where inland flows have been compromised (inferring increased SWI vulnerability). Cases 2a and 2b represent two locations with differing unconfined hydrogeological settings within the Pioneer Valley aquifer (Werner and Gallagher, 2006) whereby the setting for Case 2a was found as having increased susceptibility to SWI. Cases 3a and 3b represent the Nile Delta and Madras confined aquifer cases, respectively, studied by Sherif and Singh (1999), whereby the Nile Delta (3a) was identified as being more vulnerable to SLR and climate change-induced SWI. Case 4 represents the Uley South limestone unconfined aquifer described by Zulfic et al. (2007) and Werner et al. (2011). Cases 5 and 6 are the Qa and PWF aquifers for the Willunga Basin, respectively.

Table 4. Vulnerability indicators (Cases 1 to 4 are from Werner et al., 2012)

Case	Aquifer type	Flux-controlled			Head-controlled	
		$\frac{\partial x_T}{\partial z_0}$ (-)	$\frac{\partial x_T}{\partial W_{net}}$ (d)	$\frac{\partial x_T}{\partial q_b}$ (d/m)	$\frac{\partial x_T}{\partial z_0}$ (-)	$\frac{\partial x_T}{\partial W_{net}}$ (d)
1a	Unconfined	12	-3.8E6	-190	26	-1.9E6
1b	Unconfined	9	-5.4E6	-108	12	-2.7E6
1c	Unconfined	15	-8.8E6	-280	29	-4.3E6
2a	Unconfined	67	-2.8E6	-780	570	-1.2E6
2b	Unconfined	14	-5.9E5	-39	21	-2.9E5
3a	Confined	0	n/a	-4.7E4	9,600	n/a
3b	Confined	0	n/a	-1300	2,700	n/a
4	Unconfined	71	-3.2E6	-460	380	-1.5E6
5	Unconfined	20	-3.7E6	-770	53	-1.8E6
6	Confined	0	n/a	-9.8E5	2.6E5	n/a

Vulnerability indicator values in Table 4 can be used to rank the vulnerability of different aquifers to the same stress. It can be seen that Case 5 has a relatively low vulnerability to SLR (when compared to Cases 2a and 4) and a relatively low vulnerability to recharge change (when compared to Cases 1b and 1c). However, Case 5 has a relatively high vulnerability to changes in inflows at the inland boundary. Similarly, it can be seen that Case 6 is more vulnerable to changes in inflows at the inland boundary and SLR (for the head-controlled case) than all other cases assessed.

The vulnerability indicators cannot be used to compare sensitivities to different stresses within the same aquifer system because the indicators have different units. Werner et al. (2012) used logarithmic sensitivities in order to make this comparison. Logarithmic sensitivities measure the fractional change in output for a fractional change in a parameter (Kabala, 2001). Table 5 lists logarithmic sensitivities for Cases 1 to 6.

Table 5. Logarithmic sensitivities (after Werner et al., 2012)

Case	Aquifer type	Flux-controlled		Head-controlled		
		$\frac{\partial x_T}{\partial z_0}\frac{z_0}{x_T}$ (-)	$\frac{\partial x_T}{\partial W_{net}}\frac{W_{net}}{x_T}$ (-)	$\frac{\partial x_T}{\partial q_b}\frac{q_b}{x_T}$ (-)	$\frac{\partial x_T}{\partial z_0}\frac{z_0}{x_T}$ (-)	$\frac{\partial x_T}{\partial W_{net}}\frac{W_{net}}{x_T}$ (-)
1a	Unconfined	2.0	-1.0	-0.53	4.4	-0.5
1b	Unconfined	2.0	-1.0	-0.81	2.7	-0.5
1c	Unconfined	2.0	-1.0	-0.70	3.9	-0.5
2a	Unconfined	2.2	-1.1	-0.61	19	-0.5
2b	Unconfined	2.0	-1.0	-0.95	2.9	-0.5
3a	Confined	0	n/a	-1.0	53	n/a
3b	Confined	0	n/a	-1.0	62	n/a
4	Unconfined	2.1	-1.1	-0.82	12	-0.5
5	Unconfined	2.0	-1.0	-0.3	5.4	-0.5
6	Confined	0	n/a	-1.0	980	n/a

There is significant uncertainty regarding the designation of flux-controlled or head-controlled conditions for the Willunga Basin aquifers. However, as the Qa aquifer is not heavily utilised and is responsive to recharge, it is more likely to be flux-controlled. In contrast, the PWF and MS aquifers are heavily utilised for irrigation; therefore aquifer heads are likely to be maintained at a constant value (i.e., head controlled) by pumping despite stress changes arising from SLR or climate change. It can be seen from Table 5 that the Qa aquifer (assuming flux-controlled conditions) is more sensitive to fractional changes in SLR than to recharge change or changes in inflows at the inland boundary. For the PWF aquifer (assuming head-controlled conditions) sensitivity to SLR is significantly larger than sensitivity to changes in inflows at the inland boundary.

In general, the vulnerability indicator and logarithmic sensitivity results suggest that the key drivers of SWI in the Willunga Basin aquifers are changes in flows at the inland boundary (for the Qa and PWF aquifers) and SLR (for head-controlled conditions) in

the PWF aquifer. High vulnerability is inferred for the MS aquifer because it was found to have unstable interface conditions.

2.3.4 Transient analysis

Conceptualisation of the Willunga Basin adopted for numerical modelling of transient SWI was configured as individual representations of the Qa, PWF and MS aquifers in two dimensions, and in cross section perpendicular to the coast, as shown in Figure 5. As head-controlled settings have been shown to result in greater SLR-induced SWI within unconfined and confined aquifers compared to flux-controlled conditions (Werner and Simmons, 2009; Werner et al., 2012), all numerical model representations for this study assumed head-controlled conditions. Hence the results represent a worst case and it is assumed that heads are maintained at the same level at 3.5 km from the coast due to pumping.

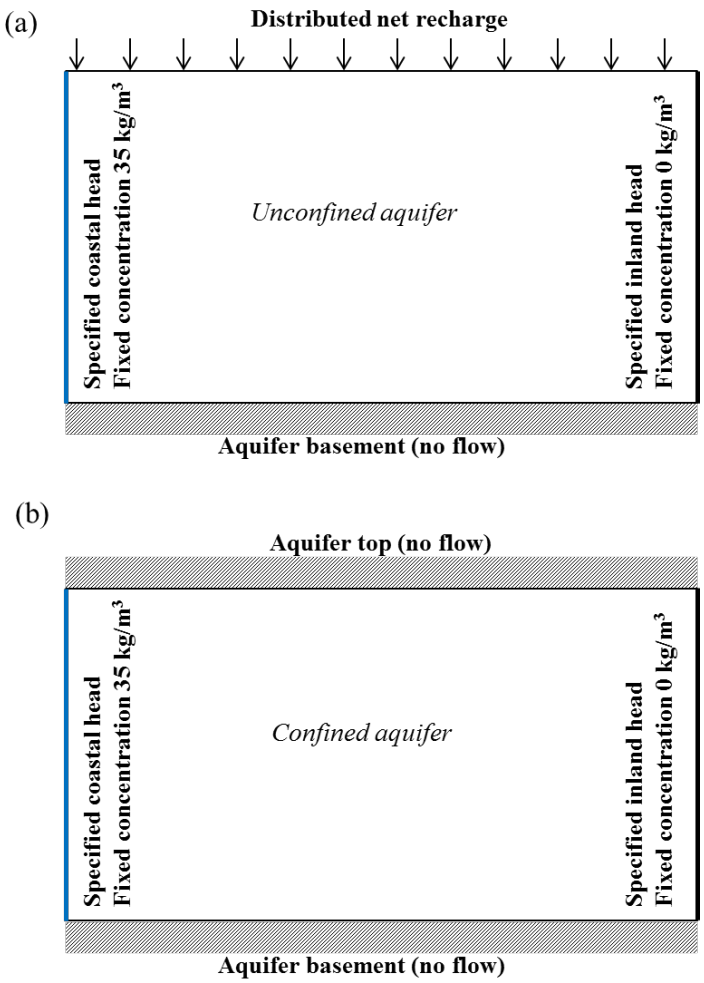

Figure 5. Simplified aquifer conceptualisations for the purposes of numerical modelling of transient SWI: (a) Qa aquifer, and (b) PWF and MS aquifers

The model domain was uniformly discretised for transient simulations of both the Qa, PWF and MS aquifers, with 700 vertical columns of 5 m width. The Qa model had 20 horizontal layers of 1 m thickness, the PWF had 36 layers of 2.5 m thickness and the MS had 26 layers of 2.5 m thickness. This grid discretisation is consistent with a Peclet number less than 2, as recommended by Diersch and Kolditz (2002) for the reduction of numerical oscillations. A specified-head boundary condition was applied at the inland boundary. A specified-head and constant-concentration boundary condition was used for the coastal boundary, with a seawater concentration of 35 kg/m^3. For confined aquifers, the coastal boundary head under initial conditions (i.e., pre-SLR) was

determined using equation (16). The Strongly Implicit Procedure (SIP) and General Conjugate Gradient (GCG) solvers were selected for flow and transport, respectively. The Hybrid Method of Characteristics (HMOC) solution scheme was selected for the advection term, with a Courant number of 0.75. A Courant number less than or equal to one is generally required to limit numerical dispersion and achieve accurate results (Zheng and Bennett, 2002).

The parameter values adopted for the numerical simulations using SEAWAT are shown in Table 6. Coastal head values are for initial conditions (i.e., pre-SLR). The assumed pre-development inland head (Table 2) was used for the PWF aquifer model so that the wedge toe under initial conditions would occur within the model domain. For the purpose of tracking SWI, the toe was defined as the interception of the 50% seawater isochlor with the aquifer basement.

Table 6. Parameter values adopted for numerical simulations using SEAWAT

		Qa	PWF	MS
Parameter (units)	Label	Value	Value	Value
Inland head (m)	h_b	3	3	2
Inland distance (m)	x_b	3500	3500	3500
Coastal head (m)		0	0.75	4
Aquifer base below sea level (m)	z_0	20	110	215
Aquifer thickness (m)	h_0	-	90	65
Recharge (mm/yr)	W_{net}	20	0	0
Horizontal hydraulic conductivity (m/d)	K_x	10	10	1
Vertical hydraulic conductivity (m/d)	K_y	10	10	10
Longitudinal dispersivity (m)	α_L	1	1	1
Transverse dispersivity (m)	α_T	0.1	0.1	0.1
Molecular diffusion (m^2/d)	D	$9E^{-5}$	$9E^{-5}$	$9E^{-5}$
Effective porosity (-)	n_e	0.3	0.3	0.3
Specific yield (-)	S_y	0.2	-	-
Specific storage (/m)	S_s	-	$2E^{-5}$	$2E^{-5}$
Seawater density (kg/m^3)	ρ_s	1025	1025	1025
Seawater salinity (kg/m^3)		35	35	35

For the parameter values in Table 6, initial steady-state conditions for the Qa and PWF aquifers were achieved using time marching, until the wedge toe was found to stabilise. Steady state was not achieved for the MS aquifer after 2000 years (for parameter values in Table 6), which is in line with previous findings (i.e., that the interface is unstable). After an initial steady state was reached for the Qa and PWF aquifers, an instantaneous SLR of 0.88 m was applied. This value is consistent with the upper value presented by the IPCC (2007) for the year 2100 and conforms to the value used in previous studies (e.g., Werner and Simmons, 2009). The effects of gradual SLR were also considered. This was achieved by applying a linear rise in sea level of 0.88 m over 90 years, consistent with the approach of Webb and Howard (2011). Results for the Qa and PWF aquifers are shown in Figures 6 and 7, respectively.

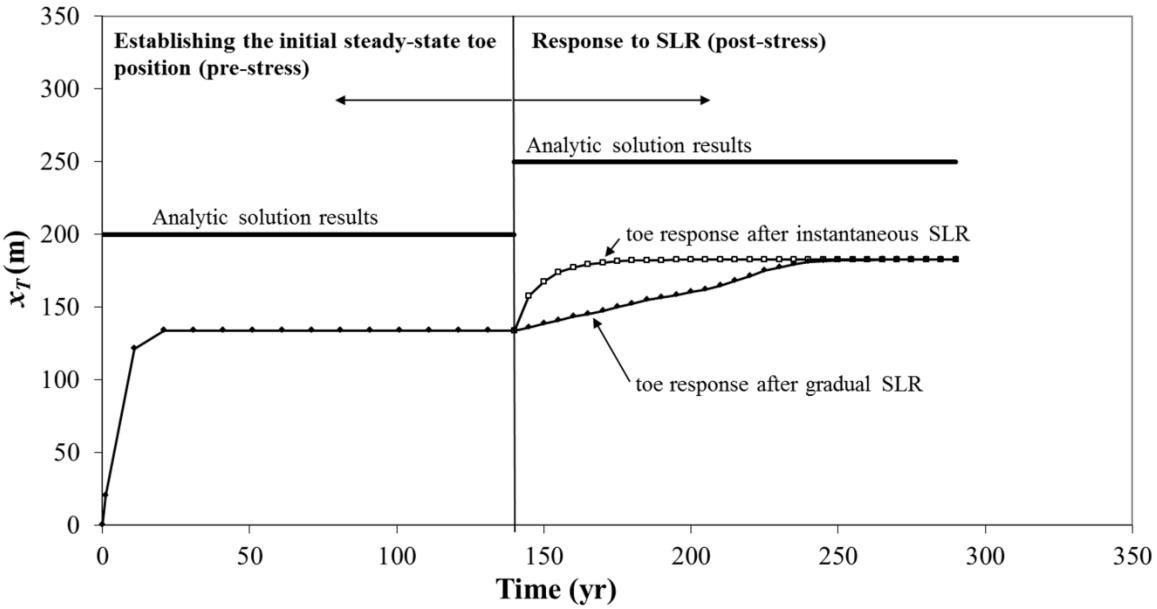

Figure 6. Comparison of toe positions in the Qa aquifer before and after SLR using the analytic, steady-state approach and transient numerical modelling

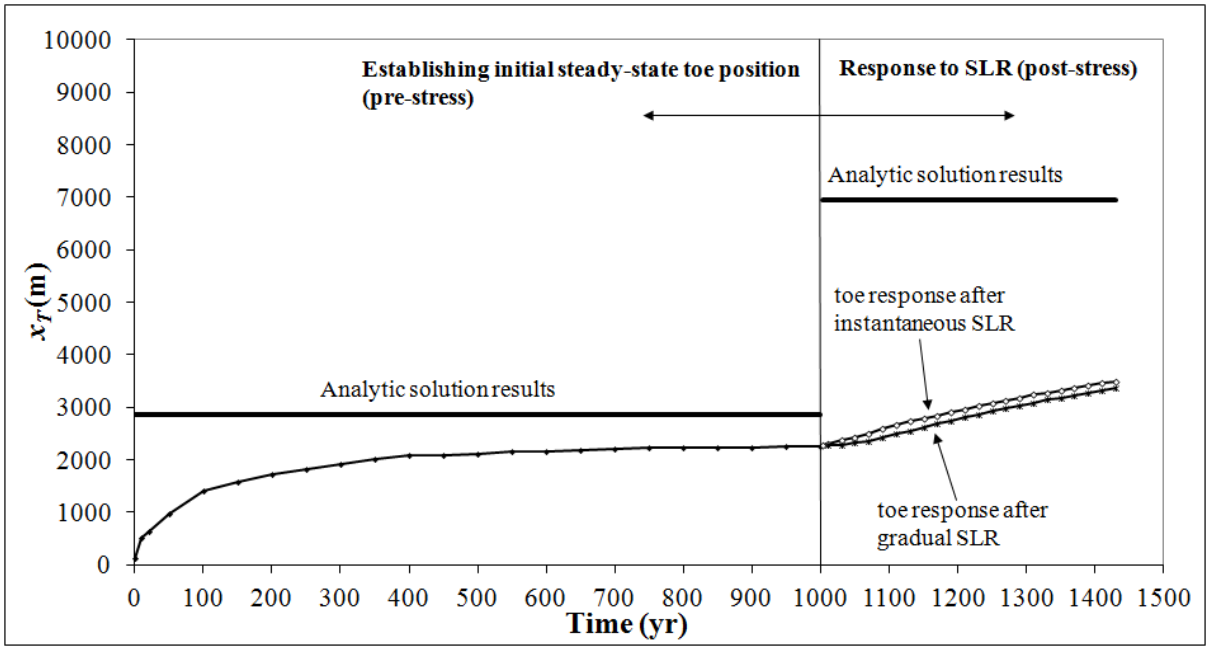

Figure 7. Comparison of toe positions in the PWF aquifer before and after SLR using the analytic, steady-state approach and transient numerical modelling

For both the Qa and PWF aquifers, x_T determined using the numerical model was less than that predicted by the analytical approach. Over-estimation of the toe by the sharp-interface method is expected (e.g., Cooper, 1964; Pool and Carrera, 2011), because the freshwater-saltwater interface is closer to the coast when the seawater circulation cell, caused by the mixing of seawater and groundwater, is considered.

Application of an instantaneous SLR to the unconfined Qa aquifer model resulted in a maximum x_T extent of around 180 m after 40 years (i.e., about a 50 m increase from pre-stress conditions). In contrast, the maximum x_T extent for the gradual SLR case was reached after approximately 100 years.

From the simulation of the PWF aquifer a steady state had not been reached after approximately 450 years in both the instantaneous and gradual SLR cases, at which time the simulation was stopped because the toe was within 50 m of the inland model boundary (x_b = 3500 m) for the instantaneous SLR case. This demonstrates that it takes a longer time for interfaces to equilibrate following SLR in the PWF than in the Qa aquifer. This is not surprising given that the PWF is more sensitive than the Qa to SLR (under head-controlled conditions) and the change in the steady-state interface position is much greater, involving larger volumes of seawater entering the aquifer. At 100 years after the commencement of SLR (a period of time relevant to management time frames), x_T had increased by about 410 m for the instantaneous rise and about 230 m for the gradual SLR.

2.4 Conclusions

A method for rapid assessment of SWI vulnerability is needed to pinpoint Australian coastal aquifers at risk of SWI and assist with prioritisation of areas where further detailed SWI investigation may be required. In this regard, the vulnerability indicators method of Werner et al. (2012) was found to be an improvement over previous methods because it is theoretically based and can be used to identify the key drivers of SWI. Also it can be applied when limited data is available. Within this study, the Werner et al. (2012) method was described through an application to the Willunga Basin, South Australia. In addition, the method was extended using a transient analysis of SLR.

The unconfined Qa aquifer was found to have relatively small SWI extent under current conditions. Comparison with cases considered previously by Werner et al. (2012) indicated that the Qa aquifer had relatively low vulnerability to SLR and recharge change and relatively high vulnerability to changes in flows at the inland boundary (as might occur under increased extraction).

The confined PWF aquifer was found to have large SWI extent under current conditions and there is the potential for a large volume of seawater to have entered (or to eventually enter) the PWF since the pre-development period. As such, active SWI is likely in the PWF aquifer. Like the Qa aquifer, the PWF aquifer was found to have a relatively high vulnerability to changes in flows at the inland boundary. Logarithmic sensitivities indicated that the PWF was most sensitive to fractional changes in SLR, assuming head-controlled conditions. In order to reduce vulnerability to SLR in the PWF aquifer, a management approach that allows heads to rise commensurate with sea-

level is required. Further detailed SWI assessment of future extraction and SLR scenarios is warranted for the PWF aquifer.

The MS aquifer was found to have unstable interface conditions, suggesting that the interface is moving inland. As such, the already high vulnerability of the MS aquifer will increase under increased stresses associated with climate change and increased extraction. Further detailed assessment of SWI extent under current conditions is required for the MS aquifer.

Transient analysis of SWI in response to a 0.88 m SLR in the Qa and PWF aquifers demonstrated that instantaneous SLR results in a more rapid SWI response than gradual SLR. For the Qa aquifer, maximum x_T extent was reached after around 40 years for instantaneous SLR and about 100 years for gradual SLR. For the PWF aquifer, a steady state had not been reached after approximately 450 years in both the instantaneous and gradual SLR cases. Instantaneous and gradual SLR results in x_T increases of about 410 m and 230 m, respectively, after 100 years.

The Willunga Basin is an important agricultural region and high priority candidate for SWI assessment. At the time of preparation of this report, the existing data set for the Willunga Basin aquifers at the coastal fringe was limited. The results of this study have provided guidance for a planned drilling program within the Willunga Basin which it is hoped will inform future SWI assessment activities.

Acknowledgements

This work was partially funded by the National Centre for Groundwater Research and Training, a collaborative initiative of the Australian Research Council and the National Water Commission.

Chapter 3

Seawater intrusion vulnerability indicators for freshwater lenses in strip islands

Abstract

Freshwater lenses on small islands are some of the most vulnerable aquifer systems in the world. However, there is currently little guidance on methods for rapidly assessing the vulnerability of freshwater lenses to the potential effects of climate change. We address this knowledge gap using a simple steady-state analytic modelling approach to develop seawater intrusion (SWI) vulnerability indicator equations, which quantify the propensity for SWI to occur in strip islands due to recharge change and sea-level rise (SLR) (incorporating the effect of land surface inundation (LSI)). The following inferences about SWI vulnerability in freshwater lenses can be made from the analysis: (1) SWI vulnerability indicators for SLR (under flux-controlled conditions) are proportional to lens thickness (or volume) and the rate of LSI and inversely proportional to island width; (2) SWI vulnerability indicators for recharge change (under flux-controlled conditions) are proportional to lens thickness (or volume) and

---

This Chapter is based on the following paper: Morgan LK, Werner AD, 2014. Seawater intrusion vulnerability indicators for freshwater lenses in strip islands, Journal of Hydrology 508, 322-327. doi:10.1016/j.jhydrol.2013.11.002.

inversely proportional to recharge; (3) SLR has greater impact under head-controlled conditions rather than flux-controlled conditions, whereas the opposite is the case for LSI and recharge change. Applications to several case studies illustrate use of the method for rapidly ranking lenses according to vulnerability, thereby allowing for prioritisation of areas where further and more detailed SWI investigations may be required.

3.1 Introduction

Rainfall recharge on oceanic islands results in a freshwater lens, whereby freshwater exists as a lens above seawater due to density differences. Freshwater lenses have been described as some of the most vulnerable aquifer systems in the world, with seawater intrusion (SWI) (i.e., the encroachment of seawater into fresh coastal aquifers) being a critical management issue (White and Falkland, 2010). Lens vulnerability has been attributed to various factors, including: (1) the generally low topographic relief of many oceanic islands, which leads to flat hydraulic gradients and high susceptibility to land surface inundation (LSI) by the ocean; (2) an often thin freshwater zone, which increases the impact of episodic droughts and excessive pumping on the lens; and (3) heavy reliance on freshwater lenses by local communities with few alternative water supplies (White et al., 2007; White and Falkland, 2010). There is significant concern regarding the potential climate-change impacts of sea-level rise (SLR) and recharge change that may compound the lens vulnerability factors described above (Mimura, 1999; Church et al., 2006; Woodroffe, 2008; White and Falkland, 2010; Terry and Chui, 2012).

SWI is a complex process and this makes SWI assessment relatively difficult and expensive (Werner et al., 2013). However, in many cases, management decision-making requires rapid and inexpensive methods for assessing vulnerability, at least as a first pass to prioritise areas where detailed SWI investigation may be required. A number of methods have been developed for rapid, large-scale SWI assessments including GALDIT (Lobo-Ferreira et al., 2007) and CVI (SLR) (Ozyurt, 2007). However, these methods largely lack a theoretical basis and instead focus subjectively on a subset of factors thought to impact SWI. For example, SWI vulnerability arising from changes in sea-level, recharge or extraction, are not captured directly, if at all, and aquifer fluxes are not accounted for.

Recently, a first-order method for assessing SWI vulnerability in continental aquifers has been developed by Werner et al. (2012), who proposed a set of theoretically based vulnerability indicators. Their method is based on the steady-state, sharp-interface equations of Strack (1976), and consequently incorporates the basic physics controlling the freshwater-saltwater interface location, albeit under idealised conditions. The premise is that partial derivative equations quantify the propensity for SWI as rates of change in SWI extent for a range of different stresses (e.g., increased extraction, reduced recharge and SLR). Using this approach, SWI vulnerability (defined as the propensity for SWI to occur) can be easily and rapidly quantified. A relatively small number of hydrogeological parameters are required for the method and this makes it suitable for application within data-poor areas. Further, SWI vulnerability to different stresses can be easily compared due to the simple nature of the underlying equations. The method was applied by Werner et al. (2012) to four coastal aquifer systems, where detailed SWI assessments have been carried out, and there was general agreement

between their approach and the vulnerability determinations obtained from more detailed investigations. Morgan et al. (2013) applied the method as part of a first-order assessment of SWI vulnerability for the multi-layered Willunga Basin aquifer system in South Australia, and offered insight into the relative vulnerability of aquifers at that site to assist with the determination of research priorities as part of an on-going field-based investigation. However, there are presently no comparable first-order SWI vulnerability methods for cases of freshwater lenses on small islands.

In this paper, we extend the work of Werner et al. (2012) to the case of freshwater lenses in islands. We focus here on the lenses of strip islands, of which there are a number of significant examples in the literature (e.g., Ghassemi, 1999; Singh and Gupta, 1999; White et al., 2007; Woodroffe, 2008). Vacher (1988) has shown that an island can be considered an infinite strip (within 1% accuracy) if the length to width ratio is greater than 2.9. The extent of SWI in the case of a freshwater lens in a strip island is characterised using both freshwater thickness at the centre of the lens and freshwater volume within the lens. SWI vulnerability indicator equations are developed that quantify the propensity for change in lens thickness and volume under recharge change and SLR. Equations are developed for both flux-controlled and head-controlled boundary conditions. This is generally consistent with the categorisation of continental coastal aquifers by Werner et al. (2012). Under flux-controlled conditions there is a no-flow boundary at the centre of the lens and the water table is able to rise or fall within the aquifer in response to SLR and recharge change. In contrast, under head-controlled conditions, the head at the centre of the island is fixed. This situation might occur, for example, due to low ground levels that control aquifer heads through increased evapotranspiration and/or runoff as the water table rises to the land surface.

Alternatively, groundwater pumping may control the water table elevation by higher pumping or increased infiltration into water supply trenches when the aquifer head increases.

Recently, Ataie-Ashtiani et al. (2013) used a simple analytic approach to assess the importance of LSI on SLR-SWI problems in unconfined continental aquifers. They showed that LSI induces significantly more extensive SWI compared to the effects of SLR where the coastal boundary is vertical. Inland penetration of seawater caused by LSI was found to be an order of magnitude greater in the worst case. For atoll islands, a number of case-specific numerical modelling studies have shown that LSI increases island vulnerability to SLR (e.g., Oberdorfer and Buddemeier, 1988; Terry and Chui, 2012). A recent generic study by Ketabchi et al. (2013) investigated the impact of SLR on freshwater lenses (assuming flux-controlled conditions) in circular and two-layer islands using analytic and numerical methods. A sensitivity analysis showed that LSI has considerable impact on fresh groundwater lenses influenced by SLR. We add to the work of Ketabchi et al. (2013) by developing SWI vulnerability indicator equations for SLR that account for the impact of LSI on (single-layer) strip islands under both flux-controlled and head-controlled boundary conditions. Finally, SWI vulnerability under recharge change and SLR (considering a range of LSI scenarios) is explored in a selection of cases.

3.2 Theory

The conceptual model used for the freshwater lens in a strip island is shown in Figure 8. The aquifer has an isotropic and homogeneous hydraulic conductivity K [L/T]. A sharp freshwater-saltwater interface and steady-state conditions are assumed. The water budget for the problem domain is comprised of net recharge W [L/T] (accounting for infiltration, evapotranspiration and distributed pumping) and freshwater discharge to the sea q_0 [L^2/T]. The hydraulic head h_f [L] is related to the depth of the interface z [L] by the Ghyben-Herzberg relation (Ghyben 1888; Herzberg 1901), such that $z = h_f / \delta$, where δ [-] is the dimensionless density $\delta = (\rho_s - \rho_f)/\rho_f$, and ρ_s and ρ_f are seawater and freshwater densities, respectively [M/L^3]. The freshwater thickness at the centre of the island (i.e., at $x = x_B$) is B [L]. The analysis assumes that SWI can be approximated as successive steady-states.

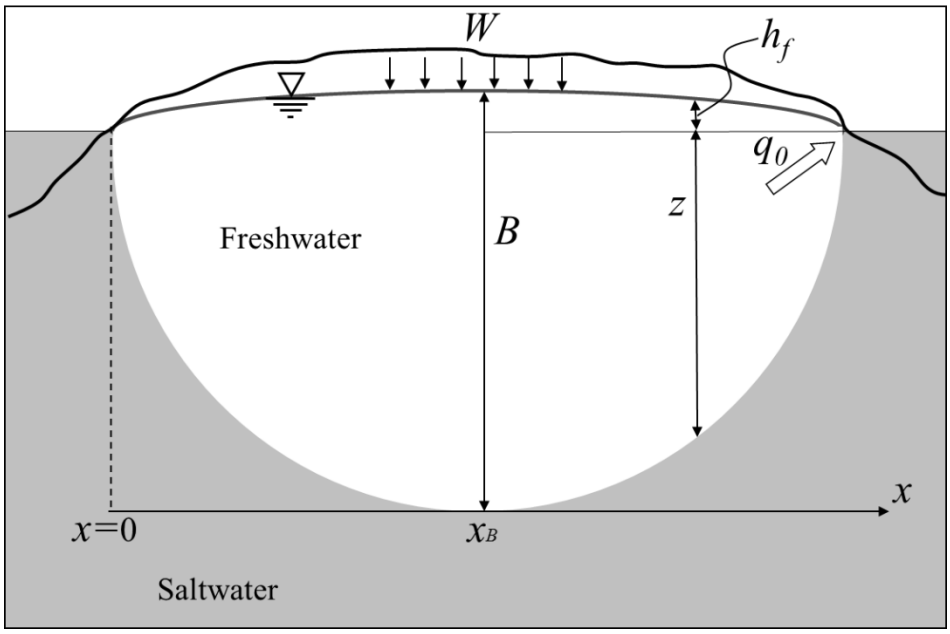

Figure 8. Conceptualisation of a freshwater lens (vertical scale exaggerated)

Strack (1976, 1989) defined the hydraulic head in a freshwater lens as:

$$h_f = \sqrt{\frac{(2q_0 x - Wx^2)}{K(1+\frac{1}{\delta})}} \tag{25}$$

3.2.1 Flux-controlled conditions

The flux-controlled case represents one where the watertable is able to rise unencumbered by land surface effects. Groundwater flow to the sea is commensurate with the total lens recharge, i.e., $q_0 = Wx_B$. Equation (25) becomes:

$$h_f = \sqrt{\frac{W(2x_B x - x^2)}{K(1+\frac{1}{\delta})}} \tag{26}$$

Equation (26) is the same as that described by Fetter (1972) for hydraulic head in a strip island lens.

Using equation (26) and the Ghyben-Herzberg approximation, the equation for the interface is:

$$z = -\frac{1}{\delta}\sqrt{\frac{W(2x_B x - x^2)}{K(1+\frac{1}{\delta})}} \tag{27}$$

The hydraulic head h_B, found at the centre of the island (i.e., where $x = x_B$), is obtained from equation (26):

$$h_B = x_B \sqrt{\frac{W}{K(1+\frac{1}{\delta})}} \tag{28}$$

From equation (28) and the Ghyben-Herzberg approximation, the freshwater thickness B (which is also the maximum freshwater thickness) is:

$$B = (1+\frac{1}{\delta})h_B = x_B \sqrt{\frac{W(1+\frac{1}{\delta})}{K}} \tag{29}$$

Freshwater volume V_{fw} [L^2] (volume is expressed per length of coastline) is obtained by integration of the difference between equations (26) and (27) and multiplying by porosity n [-]:

$$V_{fw} = n \int_0^{2x_B} (h_f - z)dx = n\frac{\pi}{2} x_B B \tag{30}$$

The numerical modelling study of Chui and Terry (2013), which employed flux-controlled conditions, found a non-linear relationship between freshwater availability and island width. Equation (30) confirms and extends these findings, showing that freshwater volume is proportional to the square of island width.

3.2.2 Head-controlled conditions

The hydraulic head is fixed at the centre of the lens due to, for example, centrally located topographic controls, surface water features or pumping, that modify the lens water balance depending on the coastal boundary head. The hydraulic head distribution is then calculated using equation (25), with q_0 given by:

$$q_0 = \frac{K}{2x_B}\frac{1+\delta}{\delta}h_B^2 + \frac{Wx_B}{2} \tag{31}$$

That is, q_0 is calculated using the known hydraulic head h_B at the centre of the island x_B. Equation (25) provides the hydraulic head distribution between $x = 0$ and $x = x_B$. Symmetry is assumed.

Using equation (25) and the Ghyben-Herzberg approximation, the equation for the interface is:

$$z = -\frac{1}{\delta}\sqrt{\frac{(2q_0 x - Wx^2)}{K(1+\frac{1}{\delta})}} \tag{32}$$

In the head-controlled case, the freshwater thickness B at the centre of the island is simply:

$$B = (1+\frac{1}{\delta})h_B \tag{33}$$

A groundwater mound (and therefore no-flow condition) may occur between the coast and the island centre (i.e., at $x = x_n$) in cases where the inland head is controlled, producing groundwater removal from the lens (assumed for simplicity to occur at x_B). In these cases, the maximum lens thickness is found at x_n (and, due to symmetry, at $2x_B - x_n$). That is, B is not necessarily the maximum lens thickness in the head-controlled case. The location of the peak of the mound is calculated using $x_n = q_0/W$, where q_0 is obtained from equation (31). The flow (out of the lens) caused by the head-controlling feature at the centre is then $2(Wx_B - q_0)$ or $2W(x_B - x_n)$.

Freshwater volume V_{fw} is obtained by integration of the difference between equations (25) and (32), and multiplying by porosity:

$$V_{fw} = n\int_0^{2x_B}(h_f - z)dx$$
$$= n\sqrt{\left(1+\frac{1}{\delta}\right)\frac{W}{K}}\left((x_B - x_n)\sqrt{2x_B x_n - x_B{}^2} + x_n^2\cos^{-1}(1-\frac{x_B}{x_n})\right) \quad (34)$$

3.2.3 Climate change stresses

3.2.3.1 Sea-level rise – flux-controlled conditions

Under flux-controlled conditions, the freshwater lens will rise commensurate with SLR. Assuming that the coastal boundary is vertical, the geometry of the lens does not change with SLR, but simply floats on the rising body of seawater (if equilibrium conditions are maintained during SLR). In this case, there is no reduction in lens thickness or freshwater volume of the lens, and hence we don't consider this to be SWI for the purposes of a vulnerability assessment. However, in some cases, oceanic islands are low lying near the shoreline and SLR will result in LSI, but the topography of the island's interior may be high enough to allow for flux-controlled conditions to persist at the centre of the island despite SLR. The propensity for B to change with SLR due to LSI is obtained by differentiating equation (29), as follows:

$$\frac{\partial B}{\partial z_0} = \frac{\partial B}{\partial x_B}\frac{dx_B}{dz_0} = \sqrt{\frac{W(1+\frac{1}{\delta})}{K}}\frac{dx_B}{dz_0} = \frac{B}{x_B}\frac{dx_B}{dz_0} \quad (35)$$

Here dx_B/dz_0 quantifies the change in island width (i.e., LSI) associated with a change in sea level z_0 [L]. dx_B/dz_0 is the inverse of the slope at the coast. Similarly, the propensity for change in V_{fw} with LSI is obtained by differentiating equation (30):

$$\frac{\partial V_{fw}}{\partial z_0} = \frac{\partial V_{fw}}{\partial x_B}\frac{dx_B}{dz_0} = n\pi B\frac{dx_B}{dz_0} = 2\frac{V_{fw}}{x_B}\frac{dx_B}{dz_0} \tag{36}$$

For the case of a vertical coastal boundary (i.e., where $dx_B/dz_0 = 0$), equations (35) and (36) indicate that B and V_{fw} are not affected by SLR, as expected. Further, the propensity for change in B due to SLR is proportional to the rate of LSI (i.e., dx_B/dz_0), under flux-controlled conditions. The propensities for changes in B and V_{fw} are proportional to B and V_{fw}, respectively, and inversely proportional to x_B. That is, a larger lens thickness (or volume) and smaller island width equate to a larger propensity for SWI due to SLR under flux-controlled conditions with LSI.

3.2.3.2 Recharge change – flux-controlled conditions

Under flux-controlled conditions, it is assumed that the no-flow boundary at the centre of the island is unchanged (i.e., flux-controlled) despite modified recharge. The propensities for changes in B and V_{fw} arising from a change in W are obtained by differentiating equations (29) and (30) with respect to W:

$$\frac{\partial B}{\partial W} = \frac{B}{2W} \tag{37}$$

$$\frac{\partial V_{fw}}{\partial W} = \frac{V_{fw}}{2W} \tag{38}$$

Equations (37) and (38) show that propensities for change in B and V_{fw} are proportional to B and V_{fw}, respectively, and inversely proportional to W. Therefore, large lenses with low recharge are most sensitive to recharge change, under flux-controlled conditions.

3.2.3.3 Sea-level rise - head-controlled conditions

It is assumed here that the head at the centre of the island h_B (which is measured relative to sea-level) reduces in proportion to the rise in sea-level. This condition can be described as:

$$\frac{\partial h_B}{\partial z_0} = -1 \tag{39}$$

Considering equations (33) and (39), the propensity for change in B in response to SLR is:

$$\frac{\partial B}{\partial z_0} = \frac{\partial B}{\partial h_B}\frac{\partial h_B}{\partial z_0} = -\frac{1+\delta}{\delta} \approx -41 \tag{40}$$

Equation (40) indicates that B will reduce by approximately 41 times any rise in sea level. This is an expected outcome given the Ghyben-Herzberg relation.

The propensity for change in freshwater volume due to SLR (without LSI) is obtained by differentiating equation (34) as follows:

$$\frac{\partial V_{fw}}{\partial z_0} = \frac{\partial V_{fw}}{\partial h_b}\frac{\partial h_b}{\partial z_0} = -n\frac{h_B}{x_B}\frac{1+\delta}{\delta}\sqrt{\frac{1+\delta}{\delta}\frac{K}{W}}$$
$$\left(-\sqrt{2x_B x_n - x_B^2} + \frac{(x_B - x_n)x_B}{\sqrt{2x_B x_n - x_B^2}} + 2x_n \arccos(1-\frac{x_B}{x_n}) - \frac{x_B}{\sqrt{1-(1-\frac{x_B}{x_n})^2}} \right) \quad (41)$$

The propensity for change in freshwater volume due to SLR with LSI is given by:

$$\frac{\partial V_{fw}}{\partial z_0} = \frac{\partial V_{fw}}{\partial h_B}\frac{\partial h_B}{\partial z_0} + \frac{\partial V_{fw}}{\partial x_B}\frac{dx_B}{dz_0}$$
$$= -n\frac{h_B}{x_B}\frac{1+\delta}{\delta}\sqrt{\frac{1+\delta}{\delta}\frac{K}{W}}$$
$$\left(-\sqrt{2x_B x_n - x_B^2} + \frac{(x_B - x_n)x_B}{\sqrt{2x_B x_n - x_B^2}} + 2x_n \arccos(1-\frac{x_B}{x_n}) - \frac{x_B}{\sqrt{1-(1-\frac{x_B}{x_n})^2}} \right)$$
$$+ n\sqrt{\frac{1+\delta}{\delta}\frac{W}{K}}$$
$$\left(\left(\frac{x_n}{x_B}\right)\sqrt{2x_B x_n - x_B{}^2} + 2x_n\left(1-\frac{x_n}{x_B}\right)\arccos(1-\frac{x_B}{x_n}) + \frac{(2x_n - x_B)}{\sqrt{1-(\frac{x_B}{x_n}-1)^2}} \right)\frac{dx_B}{dz_0} \quad (42)$$

The highly non-linear nature of equations (41) and (42) restrict simple relationships being drawn regarding propensities for SWI with SLR. These equations are applied to case studies in the following section to demonstrate their application.

3.2.3.4 Recharge change – head-controlled conditions

It is assumed here that the head at the centre of the island h_B remains constant despite recharge change. The condition can be described as:

$$\frac{\partial h_B}{\partial W} = 0 \tag{43}$$

Therefore, lens thickness at the centre of the island is independent of recharge change in this case:

$$\frac{\partial B}{\partial W} = 0 \tag{44}$$

The propensity for change in freshwater volume due to recharge change under head-controlled conditions is obtained by differentiating equation (34) with respect to *W*.

$$\begin{aligned}\frac{dV_{fw}}{dW} = {} & \frac{n}{2\sqrt{\frac{\delta KW}{1+\delta}}}\left((x_B - x_n)\sqrt{2x_B x_n - x_B{}^2} + x_n{}^2(\arccos(1-\frac{x_B}{x_n}))\right) \\ & + n\sqrt{\frac{1+\delta}{\delta WK}}\left((\frac{-x_B}{2} + x_n)\sqrt{2x_B x_n - x_B^2} + \frac{1}{2}\frac{(x_B - x_n)(x_B^2 - 2x_B x_n}{\sqrt{2x_B x_n - x_B^2}}\right) \\ & + n\sqrt{\frac{1+\delta}{\delta WK}}\left(\left(x_B x_n - 2x_n^2\right)(\arccos(1-\frac{x_B}{x_n}) + \frac{x_B x_n - \frac{x_B^2}{2}}{\sqrt{1-(-1+\frac{x_B}{x_n})^2}}\right)\end{aligned} \tag{45}$$

Equation (45) is applied to case studies in the following section to demonstrate its application.

3.3 Application to case studies

Parameter combinations from selected case studies are used to demonstrate the SWI vulnerability indicators presented above. Parameter combinations are obtained for the following cases: Case 1, Bonriki lens, Tarawa Island (White et al., 2007); Case 2, Home Island (Ghassemi et al., 1999); and Case 3, Kavaratti Island (Singh and Gupta, 1999). The influence of LSI on vulnerability is explored using three values of dx_B/dz_0 (i.e., -100, -10, -1 and 0, which are equivalent to slope angles of 0.6˚, 5.7˚, 45 ˚ and 90˚). Table 7 lists the parameters of each case. It is assumed that natural conditions, considered as flux-controlled conditions, are present in all cases prior to SLR or recharge change. Vulnerability indicators are then calculated for both flux-controlled and head-controlled conditions. Head-controlled cases adopt the h_B obtained under natural conditions as the fixed head at the centre of the island.

Table 7. Parameters, maximum freshwater thickness, freshwater volume and vulnerability indicators for three example cases.

								Flux-controlled				Head-controlled			
Case	K (m/d)	W (mm/yr)	x_B (m)	n (-)	$\frac{dx_B}{dz_0}$ (-)	B (m)	V_{fw} (m^2)	$\frac{\partial B}{\partial z_0}$ (-)	$\frac{\partial V_{fw}}{\partial z_0}$ (m)	$\frac{\partial B}{\partial W}$ (d)	$\frac{\partial V_{fw}}{\partial W}$ (md)	$\frac{\partial B}{\partial z_0}$ (-)	$\frac{\partial V_{fw}}{\partial z_0}$ (m)	$\frac{\partial B}{\partial W}$ (d)	$\frac{\partial V_{fw}}{\partial W}$ (md)
1	15	980	500	0.25	0	42.8	8.4E3	0	0	8.0E3	1.6E6	-41	-5.8E3	0	4.3E5
					-1			-0.09	-3.4E1			-41	-5.9E3	0	
					-10			-0.86	-3.4E2			-41	-6.1E3	0	
					-100			-8.6	-3.4E3			-41	-8.0E3	0	
2	20	855	250	0.3	0	17.3	2.0E3	-0	0	3.7E3	4.4E5	-41	-2.9E3	0	9.9E4
					-1			-0.07	-1.6E1			-41	-2.9E3	0	
					-10			-0.69	-1.6E2			-41	-3.0E3	0	
					-100			-6.9	-1.6E3			-41	-3.8E3	0	
3	150	330	750	0.25	0	11.8	3.5E3	0	0	6.5E3	1.9E6	-41	-8.8E3	0	5.3E5
					-1			-0.02	-9.3E0			-41	-8.8E3	0	
					-10			-0.16	-9.3E1			-41	-8.8E3	0	
					-100			-1.6	-9.3E2			-41	-9.4E3	0	

A number of inferences regarding the vulnerability of the three cases listed in Table 7 can be made. SWI vulnerability indicators for SLR and recharge change under flux-controlled conditions are generally larger (indicating higher vulnerability) when lens size is large (i.e., where B and V_{fw} are largest). Also, SWI vulnerability indicators for SLR are largest where LSI is large. These results are expected following the theoretical development in the Section 3.2.

The ranking of the cases in terms of SWI vulnerability indicators was not consistent across all indicators. While Case 1 had the highest vulnerability indicators for flux-controlled conditions, $\frac{\partial V_{fw}}{\partial W}$ (flux-controlled) was largest for Case 3. Case 3 had the highest vulnerability indicators for head-controlled conditions. This shows that vulnerability ranking may differ depending on whether flux-controlled or head-controlled conditions apply, and whether lens thickness or lens volume is used as an indicator.

Estimates of B in Table 7 are commensurate with reported values for Case 2 (16 m; Ghassemi, 1999) and Case 3 (9 m; Singh and Gupta, 1999). However, B for Case 1 is larger than the reported value (15 m; White et al., 2007). The aforementioned studies focused on the impacts of extraction on lens size, and did not consider SWI vulnerability to climate change. It is therefore not possible to directly compare the vulnerability determinations presented here to previous studies.

While the results in Table 7 allow for a vulnerability ranking of the cases, it is not possible to compare and contrast SLR and recharge changes in terms of their relative

contributions to the vulnerability of each case to SWI. That is, it isn't possible to directly compare values for $\partial B/\partial z_0$ and $\partial B/\partial W$ because these derivatives have different dimensions. One approach to facilitate this comparison is to use logarithmic sensitivities (Kabala, 2001), which measure the fractional change in an output resulting from a fractional change in a parameter. Logarithmic sensitivity of freshwater thickness under SLR, for example, is calculated as $(z_0/B)(\partial B/\partial z_0)$. In previous studies (Werner et al., 2012; Morgan et al., 2012), z_0 was the height of sea-level above an impermeable basement layer in an unconfined continental aquifer. As there is not an impermeable basement layer for strip island lenses, this definition of z_0 does not apply here. An alternative approach involves recognising that z_0 in unconfined continental aquifers is the maximum freshwater thickness below sea level. In strip islands, the maximum freshwater thickness occurs at the centre of the island (i.e., at x_B) under natural conditions, and the maximum freshwater thickness below sea-level (i.e., z_0) can be calculated as B - h_B. Table 8 lists logarithmic sensitivities for the three cases.

Logarithmic sensitivities in Table 8 demonstrated the following: (1) recharge change logarithmic sensitivities, i.e., $(W/B)(\partial W/\partial B)$ and $(W/V_{fw})(\partial W/\partial V_{fw})$, are constant values; (2) recharge change logarithmic sensitivities are largest under flux-controlled conditions; (3) SLR logarithmic sensitivities, i.e., $(z_0/B)(\partial B/\partial z_0)$ and $(z_0/V_{fw})(\partial V_{fw}/\partial z_0)$ are largest under head-controlled conditions; (4) LSI has a larger influence on logarithmic sensitivities of SLR under flux-controlled conditions than head-controlled conditions.

Table 8. Logarithmic sensitivities for 3 example cases.

		Flux-controlled				Head-controlled			
Case	$\frac{dx_B}{dz_0}$ (-)	$\frac{z_0}{B}\frac{\partial B}{\partial z_0}$ (-)	$\frac{z_0}{V_{fw}}\frac{\partial V_{fw}}{\partial z_0}$ (-)	$\frac{W}{B}\frac{\partial B}{\partial W}$ (-)	$\frac{W}{V_{fw}}\frac{\partial V_{fw}}{\partial W}$ (-)	$\frac{z_0}{B}\frac{\partial B}{\partial z_0}$ (-)	$\frac{z_0}{V_{fw}}\frac{\partial V_{fw}}{\partial z_0}$ (-)	$\frac{W}{B}\frac{\partial B}{\partial W}$ (-)	$\frac{W}{V_{fw}}\frac{\partial V_{fw}}{\partial W}$ (-)
1	0	0.0	0.0	0.5	0.5	-40	-29	0	0.1
	-1	-0.1	-0.2			-40	-29	0	
	-10	-0.8	-1.7			-40	-30	0	
	-100	-8.4	-17			-40	-40	0	
2	0	0.0	0.0	0.5	0.5	-40	-24	0	0.1
	-1	-0.1	-0.3			-40	-24	0	
	-10	-0.7	-3.3			-40	-25	0	
	-100	-6.7	-33			-40	-32	0	
3	0	0.0	0.0	0.5	0.5	-40	-29	0	0.1
	-1	0.0	-0.1			-40	-29	0	
	-10	-0.2	-1.1			-40	-29	0	
	-100	-1.6	-11			-40	-31	0	

3.4. Conclusions

In this work, SWI vulnerability indicator equations have been developed that describe the propensity for change in SWI extent for freshwater lenses in strip islands under climate change-induced SLR and recharge change. The influence of LSI under SLR was included in these equations. This work extends that of Werner et al. (2012), who developed SWI vulnerability indicators for unconfined and confined aquifer systems and did not consider LSI. Several inferences regarding SWI vulnerability in freshwater lenses can be made from the analysis: (1) SWI vulnerability indicators for SLR (under flux-controlled conditions) are proportional to lens thickness (or volume) and the rate of LSI and inversely proportional to island width; (2) SWI vulnerability indicators for recharge change (under flux-controlled conditions) are proportional to lens thickness (or volume) and inversely proportional to recharge; (3) SLR has greater impact under head-controlled conditions rather than flux-controlled conditions, whereas the opposite is the case for LSI and recharge change.

The equations were applied to three case studies to produce a ranking based on vulnerability to SLR and recharge change. Logarithmic sensitivities were used to explore the relative contributions of SLR, LSI and recharge change to SWI vulnerability. Despite the limitations of the approach that arise from the simplifying assumptions (e.g., steady-state, sharp interface, homogeneous aquifer, no outflow face), we suggest that the SWI vulnerabilities presented here provide informative first-pass estimates of the relative threats of climate change (SLR and recharge change) to the freshwater lens systems of strip islands.

Acknowledgements This work was funded by the National Centre for Groundwater Research and Training, a collaborative initiative of the Australian Research Council and the National Water Commission.

Chapter 4

On the interpretation of coastal aquifer water level trends and water balances: A precautionary note

Abstract

The changes in seawater volumes caused by seawater intrusion are often neglected in coastal aquifer management studies. The conditions under which this can result in significant water balance errors are not well understood. Interface movements also influence temporal trends in coastal aquifer water levels, but there is little guidance on this effect. In this study, we use steady-state, sharp-interface, analytic modelling to generate idealised relationships between seawater volume, freshwater volume and water levels. The approach assumes quasi-equilibrium conditions (i.e., steady-state conditions persist during temporal changes), which are evaluated using a selection of transient, dispersive simulations. The results demonstrate that seawater volume changes can influence significantly coastal aquifer water level trends, relative to the corresponding non-coastal aquifer situation, particularly within deep aquifers with high hydraulic

This Chapter is based on the following paper: Morgan LK, Werner AD, Simmons CT, 2012. A precautionary note on the interpretation of coastal aquifer water level trends and water balances, Journal of Hydrology 470-471, 280-288.

conductivity and low net recharge. It is also shown that seawater volume changes can be a significant component of coastal aquifer water balances, e.g., relative to freshwater discharge to the sea, especially within deep aquifers characterised by low hydraulic conductivity and low freshwater discharge. Transient simulations show that steady-state conditions are a reasonable approximation for a range of transient seawater intrusion situations, including two of the three cases considered in this analysis. We conclude that changes in seawater volumes should be included routinely in coastal aquifer water balances. Also, temporal trends in coastal aquifer water levels may not provide an adequate measure of freshwater storage trends. It follows that the assessment of coastal aquifer condition should consider groundwater levels relative to the hydraulic head imposed by the ocean, accounting for density effects.

4.1 Introduction

Coastal aquifers serve as major sources of freshwater in many countries (Cheng et al., 2004). Natural and anthropogenic processes that reduce freshwater discharge to the sea give rise to seawater intrusion (SWI), which causes degradation of groundwater quality through the displacement of fresh groundwater by seawater. From a water resources perspective, SWI impacts can be considered as two interlinked components (Werner et al., 2012): 1. the inland movement of seawater thereby threatening the water quality of supply wells, and 2. the loss of freshwater storage volume leading to reduced water security.

Assessing the extent of SWI, e.g., for the purposes of coastal aquifer management, requires estimation of changes in the location of the freshwater-seawater interface.

Interface characteristics used previously in SWI analyses include the distance from the coast to the seawater wedge toe (i.e., the intersection of the interface and aquifer base) and the seawater volume (i.e., volume of seawater in the seawater wedge per unit length of coastline; e.g., Werner et al., 2011; Werner et al., 2012). These characteristics (i.e., toe and seawater volume) are considered in this study as commensurate measures of the two abovementioned forms of SWI impacts, i.e., inland movements of the seawater wedge and freshwater storage losses, respectively.

The primary focus of coastal aquifer management studies is most commonly the inland movement of saltwater and associated threats to water supplies (e.g., Mantoglou, 2003; Werner and Gallagher, 2006). The loss of freshwater storage arising from SWI has received considerably less attention. In many cases, the volumes of storage loss caused by SWI are neglected in evaluating coastal aquifer water balances, despite the importance of accurate quantification of water budgets for management purposes (Bredehoeft, 2002; Custodio, 2002). The estimation of SWI-induced storage decline in practice is confounded by difficulties in quantifying interface movements, which are often poorly constrained because salinity measurements are usually sparse and infrequent. Hence, freshwater storage losses from interface movements are often undetected and subsequently not accounted for. In this study, we examine the conditions under which this may be a significant oversight in the assessment of coastal aquifer condition, i.e., where hydrograph trends are adopted as an indicator of storage depletion.

Coastal aquifer management practices in Australia highlight the issue. For example, interface movements are neglected in the coastal aquifer management investigation by

Bekesi et al. (2009), who describe the use of a groundwater level response management (GWLRM) method for the Gnangara groundwater system in Perth, Western Australia. The GWLRM method is a form of trigger-level management (Werner et al., 2011) for which Bekesi et al. (2009) calculated rates of storage change by multiplying groundwater level changes by the storage coefficient. Declines in groundwater storage of up to 1.76 Mm^3/yr were calculated for the majority of Gnangara management areas adjoining the ocean using this method. Groundwater balances for management areas were then used to identify allocation corrections. In other parts of Australia, groundwater resources are managed by comparing watertable trends to trigger values. For example, in South Australia, water allocation policies state that use of the groundwater resource cannot cause a watertable decline of greater than 0.1 m/yr, taken over the preceding 5 years (Brown et al., 2006). This applies to aquifers adjoining the ocean and where the risk of seawater intrusion has been identified. In these cases, trends in stored volumes of fresh groundwater may need to account for interface changes rather than relying on watertable decline as an independent measure of sustainability. In contrast to a non-coastal aquifer system, a reduction in freshwater volume within a coastal aquifer (e.g., in response to pumping) is manifested as both watertable decline and a displacement of freshwater via interface movements. It follows that a coastal aquifer will experience a smaller watertable decline for a given freshwater storage loss relative to a non-coastal aquifer under otherwise similar conditions. However, this effect has not been quantified in a systematic manner previously, and guidance on the relationship between storage volumes and water levels in coastal aquifers is lacking. Therefore, it is difficult to ascertain the conditions under which the influence of seawater volumes on water level trends needs to be considered, particularly in relation to management studies where aquifer conditions and trends are sought. In the case of

the Bekesi et al. (2009) analysis, freshwater storage decline is likely to have been underestimated, although the magnitude of the seawater volume effect has not been assessed.

While the influence of seawater volumes on water level trends has not been considered previously, seawater volume changes (associated with excessive groundwater pumping) have been shown to be a significant component of coastal aquifer water balances in a number of cases. For example, Larabi et al. (2008) found that for the Rmel aquifer in northern Morocco, changes in seawater volumes (estimated from numerical modelling) increased from 0 Mm^3/yr in 1973 to 2.7 Mm^3/yr in 2003. The latter volumetric change is significant relative to freshwater discharge to the sea, which was approximately 6.9 Mm^3/yr in 2003. For the Korba aquifer in north-eastern Tunisia, Kerrou et al. (2010) used numerical modelling to show that the change in seawater volume in 2004 was 8.9 Mm^3/yr. This seawater volume change was also a significant proportion of the water balance given estimates of total inflows and total outflows of 46 Mm^3/yr and 67 Mm^3/yr, respectively. Kacimov et al. (2009) report that for unconfined aquifers along the coast of Oman, changes in seawater volume per year (expressed as a percentage of the total water balance) increased from 0.3% in 1973 to 21% in 1999.

While it is clear that in the above situations seawater volume variability was an important water balance consideration, seawater volumes are neglected in assessing coastal aquifer water balances and establishing management strategies in other cases. Examples include studies by Davidson and Yu (2006), Schafer and Johnson (2009), Sun (2005), Varma (2009), Voudouris (2006) and Zulfic et al. (2007). In these cases, it was presumed that seawater intrusion represented an insignificant proportion of the overall

water balance, although no analyses were undertaken to evaluate this assumption. The conditions under which seawater volumes are an important component of the water balance of a coastal aquifer have not been explored in a general sense previously.

In this study, we undertake an evaluation of the interaction between SWI volumetric effects and watertable trends using the sharp-interface approach of Strack (1976) to ascertain whether and under what conditions watertable decline might be a potentially misleading indicator of freshwater storage losses. The study also explores the conditions under which seawater volume changes are a potentially significant component of the coastal aquifer water balance, by comparing seawater volume changes (over an assumed timeframe) to freshwater discharge to the sea. Initially, only simplified quasi-equilibrium conditions are considered, whereby the changes in the system are approximated by a shift from one steady-state to another, to provide a first-order understanding of the SWI volume effect (e.g., Werner and Simmons, 2009). This approximation allows for the application of analytical solutions and therefore a large number of situations can be assessed, providing for more comprehensive coverage of parameter combinations than possible using only transient numerical modelling. Transient simulations are used to test the quasi-equilibrium assumption for a selection of cases, and therefore build confidence in insights obtained from the analysis regarding water level-volume and volume change-water balance relationships under dynamic SWI conditions.

4.2 Theory

4.2.1 Steady-state analysis

The analytic solution developed by Strack (1976, 1989) for the steady-state location of the freshwater-seawater interface is the basis for the following analysis. Figure 9 illustrates the conceptual model. The problem domain is separated into two zones, with unconfined interface flow in zone 1 (bounded by the ocean boundary at $x = 0$ and the toe location x_T), and unconfined freshwater flow in zone 2 (i.e., inland of the interface, $x \geq x_T$).

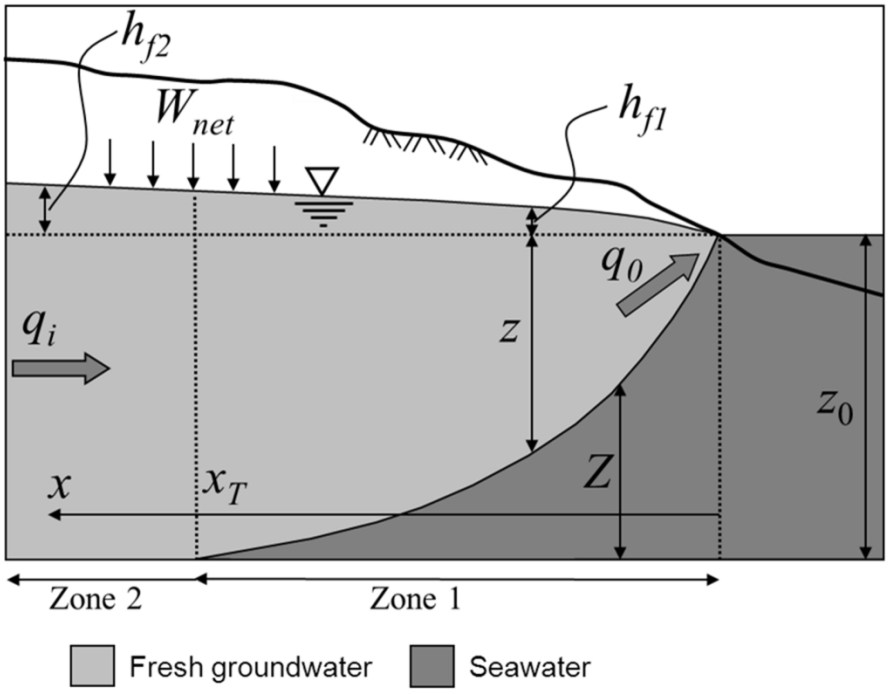

Figure 9. Conceptualisation of a steady-state sharp interface for an unconfined aquifer setting (adapted from Werner et al. (2012)).

The interface, which is z [L] below sea level, is related to the hydraulic head in zone 1 h_{f1} [L] by the Ghyben-Herzberg relation (Ghyben, 1888; Herzberg, 1901), such that $z = h_{f1}/\delta$, where δ is the dimensionless density term $\delta = (\rho_s - \rho_f)/\rho_f$, and ρ_f and ρ_s are freshwater and seawater densities [M/L^3], respectively. The interface is Z [L] above the base of the aquifer, which is obtained as $Z = z_0 - h_{f1}/\delta$, where z_0 [L] is the depth of the horizontal base of the aquifer below sea level. The discharge to the sea q_0 [L^2/T] (i.e., discharge volume per unit length of coastline per unit time, consistent with the 2D model conceptualisation) is given as $q_0 = q_i + W_{net} x_i$, where W_{net} [L/T] is distributed net recharge and q_i [L^2/T] is lateral flow exchange with the portion of the aquifer landward of the coastal fringe.

Using the method of Strack (1976, 1989), the hydraulic head in an unconfined coastal aquifer is:

$$h_{f1} = \sqrt{\left(\frac{\rho_s - \rho_f}{\rho_s}\right)\frac{2q_0 x - W_{net} x^2}{K}} \qquad \text{(Zone 1: } x \le x_T\text{)} \qquad (46)$$

$$h_{f2} = \sqrt{\frac{2q_0 x - W_{net} x^2}{K} + \left(\frac{\rho_s}{\rho_f}\right) z_0^2} - z_0 \qquad \text{(Zone 2: } x \ge x_T\text{)} \qquad (47)$$

Here, K is the hydraulic conductivity [L/T]. The value for q_0 can be determined using equations (46) and (47) in combination with a head level measurement at some distance from the coast. Through substituting $h_{f1} = \delta z_0$ and $x = x_T$ in equation (46), the following relation for the location of the wedge toe is obtained (Cheng and Ouazar, 1999):

$$x_T = \frac{q_0}{W_{net}} - \sqrt{\left(\frac{q_0}{W_{net}}\right)^2 - \frac{K\delta(1+\delta)z_0^2}{W_{net}}} \quad (W_{net} > 0) \tag{48}$$

Integration of the interface height above the aquifer basement over the interval $0 \le x \le x_T$ produces the equation for the steady-state seawater volume within an unconfined coastal aquifer (Werner et al., 2012):

$$V_{sw} = n_e \int_0^{x_T} Z dx = n_e z_0 \left(x_T - \frac{x_n}{2} \left(\sqrt{\frac{1}{M}} \arcsin\left(\sqrt{M}\right) - \sqrt{1-M} \right) \right) \tag{49}$$

Here, n_e [-] is effective porosity, and x_n [L] is the inland distance to the no flow boundary, given by $x_n = q_0 / W_{net}$. Werner et al. (2012) adopted a mixed convection ratio *M*, defined as:

$$M = \frac{K\delta(1+\delta)z_0^2}{W_{net} x_n^2} \tag{50}$$

The numerator of *M* reflects density-driven processes that cause the interface to penetrate further landward. The denominator of *M* accounts for freshwater advection that opposes the inland migration of the wedge. When *M* = 1, the wedge toe has penetrated inland to the no-flow boundary and, as such, the interface has reached an unstable condition whereby the interface will continue to penetrate inland and will fully penetrate the aquifer at steady-state. As such, *M* = 1 is an instability limit and when *M* > 1 the interface is unstable.

The freshwater volume V_f [L^2] (volume is expressed per length of coastline) in the unconfined coastal aquifer is found by integrating the thickness of the freshwater within

the aquifer between $x = 0$ and $x = x_a$, where x_a [L] is a somewhat arbitrary inland distance over which volumes are considered (taken as the aquifer's inland extent in this study), and is independent of x_n and x_T. In zone 1, the freshwater thickness is given by $h_{f1} + z_0 - Z$, and in zone 2 it is given by $h_{f2} + z_0$. Therefore, the freshwater volume is given by:

$$V_f = n_e\left(\int_0^{x_T} h_{f1}dx + \int_{x_T}^{x_a} h_{f2}dx + z_0 x_a - \int_0^{x_T} Zdx\right) \tag{51}$$

where:

$$\int_0^{x_T} h_{f1}dx = \frac{1}{2}\sqrt{\frac{\delta W_{net}}{(1+\delta)K}}\left[\left((x_T - x_n)\sqrt{2x_T x_n - x_T^2} + x_n^2 \arccos(1-\frac{x_T}{x_n})\right)\right] \tag{52}$$

and:

$$\begin{aligned}\int_{x_T}^{x_a} h_{f2}dx =& z_0(x_T - x_a) + \\ &\frac{1}{2}\sqrt{\frac{W_{net}}{K}}\left((x_a - x_n)\sqrt{\frac{x_n^2}{\delta}M - x_a{}^2 + 2x_n x_a} + x_n^2(1+\frac{M}{\delta})\arcsin\left(\frac{x_a - x_n}{x_n\sqrt{(1+\frac{M}{\delta})}}\right)\right) - \\ &\frac{1}{2}\sqrt{\frac{W_{net}}{K}}\left((x_T - x_n)\sqrt{\frac{x_n^2}{\delta}M - x_T{}^2 + 2x_n x_T} + x_n^2(1+\frac{M}{\delta})\arcsin\left(\frac{x_T - x_n}{x_n\sqrt{(1+\frac{M}{\delta})}}\right)\right)\end{aligned} \tag{53}$$

The freshwater volume within the coastal aquifer is then obtained by substituting equations (52), (53) and (49) into equation (51) for the respective integral terms. The freshwater volume equations developed within this section have not been described within the literature previously.

The potential magnitude of the impact of seawater volumes on water level decline will be examined by comparing coastal (i.e., marine) and non-coastal (i.e., freshwater and no SWI) conditions, in terms of the change in the equilibrium groundwater level in both systems in response to a reduction in freshwater storage. The non-coastal situation analysed here is one where the ocean boundary in Figure 9 is replaced by a constant freshwater boundary, e.g., as might be imposed by a lake, river or other fresh surface water body. The non-coastal problem is one of constant density and as such SWI does not displace freshwater.

Using the method of Strack (1989), the equation for the hydraulic head h_f in a freshwater-only system is given by:

$$h_f = \sqrt{\frac{-W_{net}x^2}{K} + \frac{2q_0 x}{K} + z_0^{\,2}} - z_0 \tag{54}$$

In practice, the value for q_0 can be estimated through rearranging equation (54) and applying a measured head level at a known distance from the freshwater boundary. The freshwater volume V_f is found by integrating the freshwater thickness between $x = 0$ and $x = x_a$, as:

$$V_f = n_e \left(\int_0^{x_a} (h_f + z_0) dx \right) \tag{55}$$

After substituting equation (54) into equation (55) and integrating, we obtain:

$$V_f = \frac{n_e}{2}\sqrt{\frac{W_{net}}{K}}\left((x_a - x_n)\sqrt{\zeta^2 - (x_a - x_n)^2} + \zeta^2 \arcsin\left(\frac{x_a - x_n}{\zeta}\right)\right) - \frac{n_e}{2}\sqrt{\frac{W_{net}}{K}}\left(- x_n\sqrt{\zeta^2 - (-x_n)^2} + \zeta^2 \arcsin\left(\frac{-x_n}{\zeta}\right)\right) \tag{56}$$

Here, $\zeta = \sqrt{\frac{Kz_0^2}{W_{net}} + x_n{}^2}$.

The analysis of the non-coastal case that follows involves freshwater volume reductions that may cause the watertable to intersect the base of the aquifer, at $x < x_a$. The watertable intersects the base of the aquifer at some point inland of the no-flow boundary (i.e., x_n), because $h_f + z_0$ reduces with x, according to equation (54). Where this occurs within the region of interest, i.e., $x < x_a$, the freshwater volume is obtained from equation (55) by applying an upper integration limit of $x = x_n + \sqrt{x_n{}^2 + Kz_0^2 / W_{net}}$, which is the location at which the watertable and aquifer basement intersect. In this case the freshwater volume is given by:

$$V_f = \frac{n_e}{2}\sqrt{\frac{W_{net}}{K}}\left[x_n \sqrt{\frac{Kz_0^2}{W_{net}}} + \zeta^2 \left(\arccos\left(\frac{-x_n}{\zeta^2} \right) \right) \right] \quad (57)$$

4.2.2 Transient analysis

The quasi-equilibrium assumption (i.e., steady-state conditions persist during temporal changes) of the steady-state analysis is explored in the following using transient 2D numerical modelling. The variable-density flow and solute transport code SEAWAT Version 4 (Langevin et al., 2008) was used. Description of the numerical methods and equations used in SEAWAT can be found in Guo and Langevin (2002) and Langevin et al. (2008), and are not repeated here for brevity.

4.3 Application of Theory

4.3.1 Steady-state analysis

The relationships between changes in freshwater storage and both watertable trends (within coastal and non-coastal aquifers) and changes in seawater volume (within coastal aquifers) were examined through application of the theory described in Section 4.2.1. Three base cases were adopted that comprise published parameter values, as described below. Sensitivity analyses involving a selection of parameter combinations were used to examine both the general nature of water level–volume relationships and the relative contribution of seawater volume changes to the coastal aquifer water balance.

The analysis assumed quasi-equilibrium conditions, and therefore the results are approximate. This assumption was tested using transient numerical modelling, as described in Section 4.3.3. The water balance analyses adopted a given timeframe to convert changes in seawater volume to fluxes, which were compared to rates of freshwater discharge to the sea. That is, it was assumed that a 2 m change in water level (arbitrarily at 2 km from the coast) occurred during a 20-year timeframe (i.e., a water level decline of 0.1 m/yr, reflecting observed rates for the base cases described later in this section).

Parameters for three base cases were taken from the SWI vulnerability study by Werner et al. (2012), and are shown in Table 9. Case 1 parameters apply to the Gaza coastal aquifer in Palestine (Moe et al., 2001), Case 2 parameters represent the Pioneer Valley

in Queensland, Australia (Werner and Gallagher, 2006), and Case 3 parameters are based on the Uley South basin in South Australia (Zulfic et al., 2007). In Table 9, the water levels h_b^* at x_b = 2 km from the coast (where x_b is the distance from the coast to the inland location at which water levels are determined) reflect recent conditions, as reported for each case. The asterisk is used to differentiate observed values from h_b values used or calculated in the analyses. An inland aquifer extent of x_a = 5 km was selected arbitrarily for all cases. One case using x_a = 10 km was also considered to show the influence of x_a on the results. An effective porosity of 0.3, typical of values for well-sorted sand (Fetter, 2001), was adopted for all cases (in the absence of reported values).

Table 9. Parameter values adopted for the base cases (from Werner et al. (2012)).

Case	K (m/d)	W_{net} (mm/yr)	z_0 (m)	δ (–)	x_b (km)	h_b^* (m)
1	15	31	100	0.025	2	3.7
2	100	110	25	0.025	2	1
3	200	100	25	0.025	2	1

For the cases listed in Table 9, V_f was calculated using equations (30), (35) and (36) for the coastal and non-coastal systems. V_{sw} was calculated using equation (28). Relationships between V_f, V_{sw} and h_b were determined by calculating both V_{sw} and h_b at V_f increments of 50 m^2 (volume per metre of coastline). The ratio of incremental change in V_{sw} to incremental change in V_f (i.e., $\Delta V_{sw}/\Delta V_f$) was adopted as a measure of the relative importance of seawater in reducing the freshwater storage of the aquifer during water level decline. To determine these relationships over a larger range of V_f, V_{sw} and h_b values, values of h_b were initially set to 2 m above h_b^* values listed in Table 9. The instability limit (M = 1) also restricted the allowable range of parameter testing.

The significance of ΔV_{sw} as a water balance component was assessed through comparison with q_0, for cases listed in Table 9. This comparison was enabled by converting ΔV_{sw} [L^2] to a rate of seawater volume change, using an assumed time scale Δt [T] of 20 years (i.e., $\Delta V_{sw}/\Delta t$). ΔV_{sw} was calculated following a reduction in h_b of 2 m (from the starting value of $h_b = h_b^* + 2$ m). That is, it was assumed that h_b declines at 0.1 m/yr for 20 years, and that quasi-equilibrium conditions persist (i.e., for the water level and interface distributions). While this time scale and change in h_b were selected somewhat arbitrarily, they reflect rates of decline similar to those reported for a number of coastal aquifers, including Case 1, the Gaza aquifer (1.9 m over 17 years; Qahman and Larabi, 2006) and Case 3, the Uley South aquifer (2 m over 20 years; Zulfic et al., 2007). The ratio $\omega = \Delta V_{sw} / q_0 \Delta t$ (where q_0 is calculated after the reduction in h_b) was defined as an indicator of the significance of seawater volume changes within the water balance.

4.3.2 Sensitivity analysis

A sensitivity analysis of the water level–volume relationship (i.e., the relationship between V_f, V_{sw} and h_b) and the volume change–water balance relationship (i.e., ω) was carried out using Case 3 as a base case. Combinations of typical values of K (5 m/d, 20 m/d, 200 m/d), z_0 (25 m, 50 m, 100 m) and W_{net} (1 mm/yr, 10 mm/yr, 50 mm/yr, 100 mm/yr) were used, consistent with the collective range of parameters reported by Moe et al. (2001), Werner and Gallagher (2006), Zulfic et al. (2007), Kacimov et al. (2009), Kerrou et al. (2010) and Watson et al. (2010).

The water level-volume relationship was quantified using the area between the coastal and non-coastal water level curves, as demonstrated in Figure 10. A reduction in V_f of 5000 m^2 was considered. The instability limit (M = 1) was not reached in all cases. This area, β [L^3], was used as an indicator of the influence of seawater volumes on water level trends within coastal aquifers, under conditions of declining freshwater volumes. That is, larger β values identified aquifers in which water level trends were most affected by changes in seawater volumes.

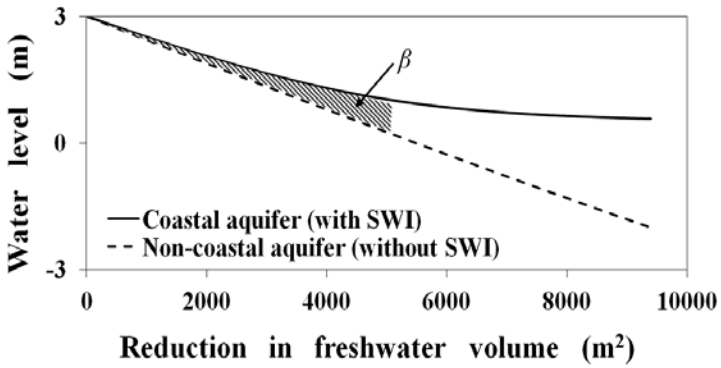

Figure 10. Comparison between water level-volume relationships for coastal and non-coastal aquifers.

Sensitivity of the volume change-water balance relationship was assessed for a change in h_b from 3 m to 2.5 m. This change was smaller than that used in Section 3.3.1 to avoid instability (i.e., $M \geq 1$) within the 36 parameter combinations considered as part of the sensitivity analysis. A five-year time scale was assumed, corresponding to a water level decline rate of 0.1 m/yr, consistent with the rate of decline used previously (Section 4.3.1).

4.3.3 Transient analysis

The assumption of quasi-equilibrium conditions persisting in the watertable and interface distributions was tested using 2D dispersive modelling of the three base cases given in Table 9. Parameter values are listed in Table 10. The analysis was carried out by comparing the transient and steady-state toe locations, both determined using SEAWAT, during and following a 0.1 m/yr decline in inland head over 20 years (a rate of decline consistent with the steady-state analysis). A small difference between the steady-state and transient toe positions indicated that quasi-equilibrium interfaces were a reasonable approximation of transient SWI.

Table 10. Parameter values adopted for numerical simulations.

		Case 1	Case 2	Case 3
Parameter (units)	Symbol	Value	Value	Value
Initial inland head (m)	h_b	5.7	3	3
Final inland head (m)	h_b*	3.7	1	1
Period of water level decline (yr)	t	20	20	20
Aquifer depth below sea level (m)	z_0	100	25	25
Recharge (mm/yr)	W_{net}	31	110	100
Horizontal hydraulic conductivity (m/d)	K_x	15	100	200
Vertical hydraulic conductivity (m/d)	K_y	15	100	200
Model length (m)		2000	2000	2000
Longitudinal dispersivity (m)	α_L	10	10	10
Transverse dispersivity (m)	α_T	0.1	0.1	0.1
Molecular diffusion (m^2/d)	D	0	0	0
Effective porosity (-)	n_e	0.3	0.3	0.3
Specific yield (-)	S_y	0.2	0.2	0.2
Seawater density (kg/m^3)	ρ_s	1025	1025	1025
Seawater salinity (mg/L)		35,000	35,000	35,000

The cross-sectional model domain was uniformly discretised for transient simulations using 400 vertical columns of 5 m width, and 110 horizontal layers of 1 m thickness (Case 1) or 30 layers of 1 m thickness (Cases 2 and 3). The inland water level remained

constant for 130 years following the 20-year period of watertable decline. A head-dependent flux boundary condition (i.e., a general head boundary) was used at the inland boundary to overcome issues of dry cells that violate SEAWAT's assumption of saturated conditions (a high hydraulic conductance (1000 m^2/d) was used to approximate a specified head condition). A check of head values at the general head boundary showed that they were within 10^{-3} m of the specified values over the duration of the simulations. The coast was simulated using Dirichlet boundary conditions for head and concentration, with a seawater concentration of 35,000 mg/L. The Strongly Implicit Procedure and General Conjugate Gradient solvers were selected for flow and transport calculations, respectively (Guo and Langevin, 2002). The Total-Variation Diminishing advection package was used with a courant number of 0.75, where a courant number less than or equal to one is generally required to limit numerical dispersion and achieve accurate results (Zheng and Bennett, 2002). The initial conditions for all simulations were taken as the steady-state conditions attained through long-term (approximately 2000 years) transient simulations. It was assumed that steady-state had been reached when the position of the toe was within 0.1 m of the final position over the 150-year simulation period. The toe was defined as the point of interception of the 5% seawater isochlor with the aquifer basement.

Case 3 was used as the base case for a small number of additional simulations aimed at exploring the conditions under which disequilibrium occurs with a change of inland head. General guidance on disequilibrium associated with inland head changes is not available in the literature, although Webb and Howard (2010) considered disequilibrium associated with sea-level rise, finding it to be greatest for the largest changes in seawater volume, i.e., high K, low W_{net} and high n_e. Specific yield and

specific storage were found to have little effect and z_0 was not assessed. As an extension to Webb and Howard's (2010) study, the influence of K, W_{net}, n_e and z_0 on disequilibrium arising from an inland head change was assessed using the following parameter values: K (20 m/d, 50 m/d, 200 m/d), W_{net} (1 mm/yr, 100 mm/yr, 200 mm/yr), n_e (0.1, 0.3) and z_0 (10 m, 25 m). Disequilibrium was quantified using the time to steady-state (i.e., lag time) following the decline of inland head.

4.4 Results

4.4.1 Water level – volume relationship

The relationships between V_f, V_{sw} and h_b for Cases 1 to 3 (Table 9) are shown in Figure 11. As V_f reduces, $\Delta V_{sw}/\Delta V_f$ approaches -1 asymptotically for each case. That is, as SWI progresses, a condition approaches whereby an incremental reduction in V_f causes an almost equivalent increase in V_{sw}, and h_b is insensitive to changes in V_f. Conversely, for low values of V_f decline, the value of $\Delta V_{sw}/\Delta V_f$ is relatively low because the degree of SWI in the system is small and an incremental change in freshwater volume results in a relatively small change in seawater volume. This is illustrated by the coastal and non-coastal aquifer water level-volume curves in Figures 11a, 11c, 11e and 11g. For a 15% reduction in V_f in Cases 1, 2 and 3 (equal to ΔV_f values of about 23,000 m^2, 6300 m^2 and 6350 m^2, respectively), $\Delta V_{sw}/\Delta V_f$ varies significantly (from -0.40 to -0.92 in Case 1, and -0.10 to -0.75 in Cases 2 and 3). As such, water levels are increasingly insensitive to changes in V_f. In general terms, situations involving water levels that are insensitive to freshwater storage change are characterised by high M

values, e.g., M values are in the range 0.39 to 0.67 (calculated after the V_f decline of 15% in the cases tested).

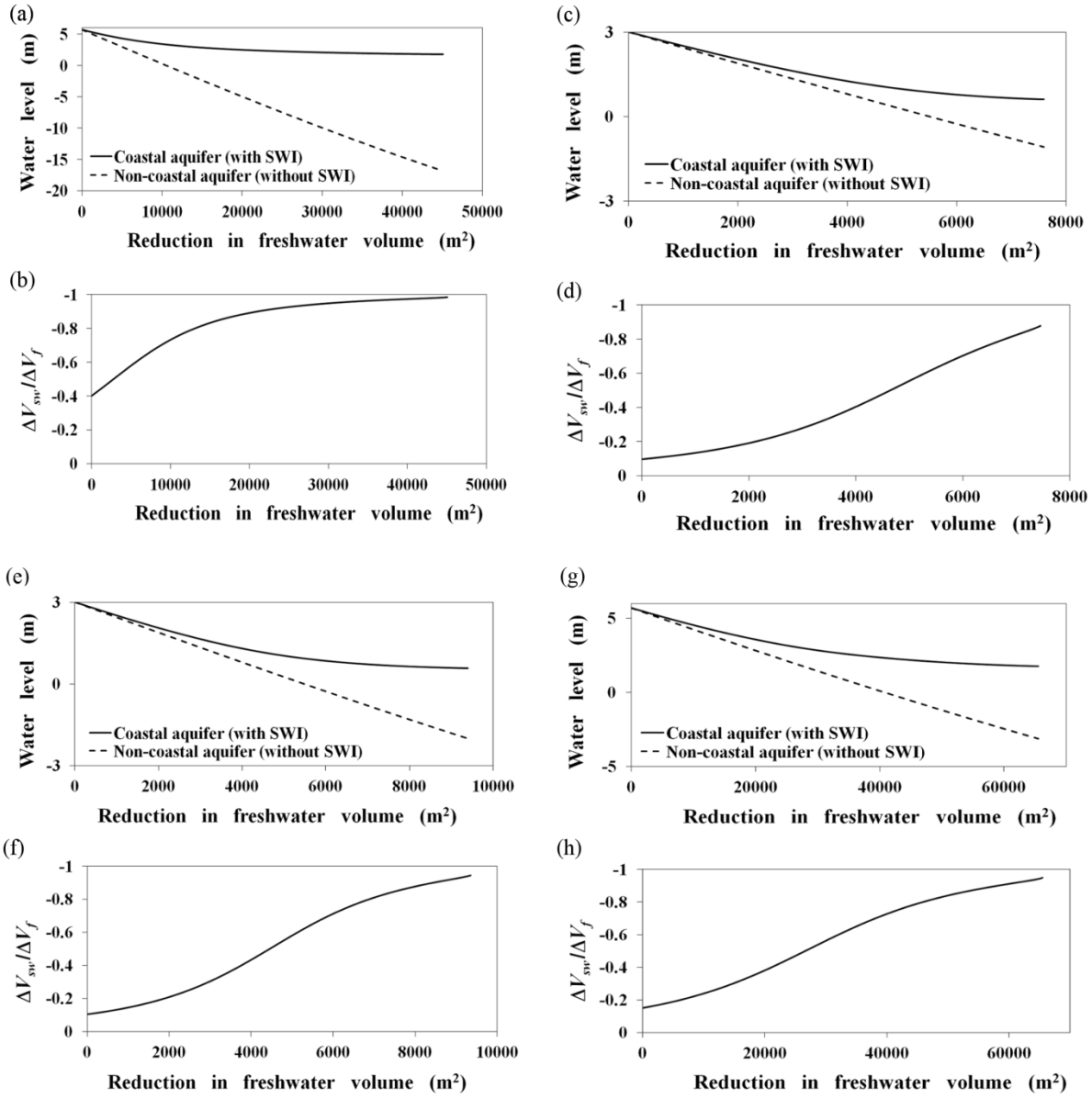

Figure 11. Water level-volume relationships: (a) Water level versus ΔV_f for Case 1, (b) $\Delta V_{sw}/\Delta V_f$ versus ΔV_f for Case 1, (c) Water level versus ΔV_f for Case 2, (d) $\Delta V_{sw}/\Delta V_f$ versus ΔV_f for Case 2, (e) Water level versus ΔV_f for Case 3, (f) $\Delta V_{sw}/\Delta V_f$ versus ΔV_f for Case 3, (g) Water level versus ΔV_f for Case 1 with x_a = 10 km, (h) $\Delta V_{sw}/\Delta V_f$ versus ΔV_f for Case 1 with x_a = 10 km.

Case 1 was assessed for inland aquifer extents of x_a = 5 km (Figures 11a and 11b) and x_a = 10 km (Figures 10g and 10h). The value of $\Delta V_{sw} / \Delta V_f$ is closer to -1 for the x_a = 5 km case over equivalent reductions in V_f, indicating that V_{sw} is a larger component of V_f decline in this case, as expected. Also, the influence of V_{sw} on water level trends is smaller for x_a = 10 km. These results indicate that water levels are less sensitive to changes in V_f within coastal aquifers with greater inland extent; an intuitive result.

4.4.2 Seawater volumes in the water balance

The significance of changes in seawater volumes within the water balance was assessed using the ratio of seawater volume rates of change to coastal discharge, given as $\omega = \Delta V_{sw} / q_0 \Delta t$ in Section 4.3.1, as shown in Table 11. For Cases 1, 2 and 3, a 2 m drop in water levels (over 20 years) results in ω values of 0.31, 0.15 and 0.10, respectively. These values are comparable to real-world observations. For example, Larabi et al. (2008) quoted ω values in the order of 0.39. Clearly, changes in V_{sw} due to interface movements can be a significant component of coastal aquifer water balances. The conditions under which this occurs are examined in Section 4.4.3. As distinct from the water level–volume relationship, ω values are independent of x_a. This occurs because V_{sw} and q_0 (defined in Section 4.2.1) are independent of x_a.

Table 11. Volume change-water balance results.

Case	$\Delta V_{sw} / \Delta t$ (m^2/d)	q_0 (m^2/d)	ω (-)
1	0.6	2.0	0.31
2	0.2	1.2	0.15
3	0.2	2.1	0.10
1[a]	0.6	2.0	0.31

[a] Case 1 with x_a = 10 km

4.4.3 Sensitivity analysis

Results of the sensitivity analysis of the water level–volume relationship are presented in Table 12 (over page). These results (combined with those of Cases 1 and 2) indicate that for unconfined aquifers, V_{sw} has greatest influence on water level trends (as quantified by β) within aquifers with high z_0, high K and low W_{net} (in relative terms). Water level trends in aquifers of this type need to account for seawater volume changes to avoid underestimation of freshwater volume changes.

The parameter combinations in Table 12 (and Cases 1 and 2) produce ω values ranging between 0.01 and 9.72. Higher ω values (representing more significant seawater volume changes in the water balance) are obtained for aquifers with high z_0, low K and low W_{net}. In general, changes in V_{sw} can be a significant water balance component (e.g., relative to q_0), thus highlighting the need to consider freshwater storage losses due to SWI when developing coastal aquifer water budgets, at least for the system characteristics adopted here.

Table 12. Sensitivity analysis parameter sets and results.

Parameter Set	K (m/d)	z_0 (m)	W_{net} (mm/yr)	β (m^3)	$\Delta V_{sw} / \Delta t$ (m^2/d)	q_0 (m^2/d)	ω (-)
1	5	25	1	20.6	0.07	0.15	0.50
2	5	25	10	16.0	0.05	0.17	0.32
3	5	25	50	9.8	0.02	0.28	0.08
4	5	25	100	1.8	0.01	0.40	0.03
5	5	50	1	38.0	0.38	0.25	1.53
6	5	50	10	36.0	0.34	0.27	1.26
7	5	50	50	27.3	0.20	0.38	0.52
8	5	50	100	17.3	0.11	0.52	0.22
9	5	100	1	61.2	3.14	0.32	9.72
10	5	100	10	57.6	3.06	0.35	8.81
11	5	100	50	56.1	2.62	0.46	5.74
12	5	100	100	51.1	2.05	0.59	3.45
13	20	25	1	21.0	0.07	0.58	0.13
14	20	25	10	19.8	0.07	0.60	0.12
15	20	25	50	14.9	0.05	0.72	0.07
16	20	25	100	9.9	0.04	0.85	0.04
17	20	50	1	38.1	0.38	0.98	0.39
18	20	50	10	37.6	0.37	1.00	0.37
19	20	50	50	35.4	0.32	1.11	0.29
20	20	50	100	32.7	0.27	1.25	0.21
21	20	100	1	58.0	3.14	1.28	2.45
22	20	100	10	57.9	3.12	1.31	2.38
23	20	100	50	57.5	3.01	1.42	2.12
24	20	100	100	57.1	2.90	1.55	1.86
25	200	25	1	21.1	0.08	5.75	0.01
26	200	25	10	21.0	0.07	5.78	0.01
27	200	25	50	20.5	0.07	5.95	0.01
28 [a]	200	25	100	19.8	0.07	6.08	0.01
29	200	50	1	38.2	0.39	9.66	0.04
30	200	50	10	38.1	0.39	9.68	0.04
31	200	50	50	37.9	0.38	9.84	0.04
32	200	50	100	37.6	0.37	9.96	0.04
33	200	100	1	58.0	3.14	12.8	0.25
34	200	100	10	58.0	3.14	12.8	0.24
35	200	100	50	57.9	3.14	12.9	0.24
36	200	100	100	57.9	3.12	13.1	0.24

[a] Base case

4.4.4 Transient analysis

Results of the transient analysis are presented in Figure 12. There is a relatively large difference between the steady-state and transient toe locations for Case 1 during the first 80 years of the 150-year simulation period. This indicates that the assumption of quasi-equilibrium conditions persisting between the watertable and interface is questionable, at least at early times, in this case. However, for Cases 2 and 3, there is relatively little difference between the transient and steady-state toe locations, demonstrating that the quasi-equilibrium assumption is valid for both of these cases.

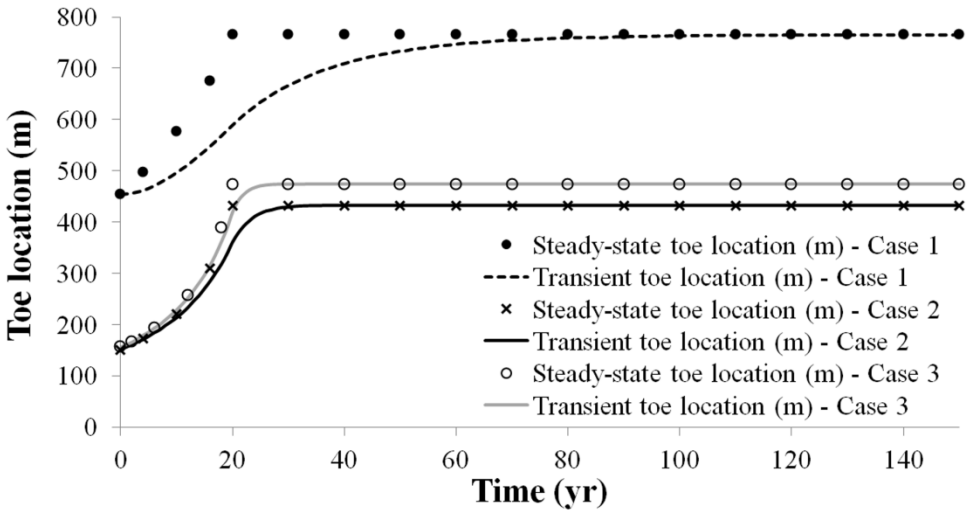

Figure 12. Comparison of transient and steady-state x_T for an inland head decline of 2 m over 20 years.

A small number of transient simulations (see Section 4.3.3) were also carried out to explore the general conditions under which disequilibrium occurs for a decline of inland head. Disequilibrium was found to be greatest for low K, high n_e and large z_0 (results not shown for brevity). These results explain the higher level of disequilibrium in Case 1, which (compared to Cases 2 and 3) had relatively low K (i.e., 31 m/d) and large z_0

(i.e., 100 m). W_{net} was found to have little effect for the parameter values (i.e., 1 mm/yr to 200 mm/yr) considered. These results indicate that the assumption of quasi-equilibrium conditions is likely to be valid for shallow unconfined aquifers with high K and low n_e. These disequilibrium results are compared to previous studies in Section 4.5.1.

4.5 Discussion

4.5.1 Transient analysis

Webb and Howard (2010) found greatest disequilibrium for high K aquifers (as described in Section 4.3.3), in contradiction to our findings (Section 4.4.4). This suggests different controls on disequilibrium associated with changes of sea level and inland head, with disequilibrium in the latter likely a function of both magnitude of change in seawater volume and change in freshwater flux. This conforms to the concept of characteristic time described by van Dam (1999), i.e., the ratio of change in seawater volume to change in freshwater flux, where large characteristic times equate to large SWI lag times and disequilibrium. Given the limited number of simulations, further research is needed to systematically evaluate relationships between disequilibrium, lag times and aquifer characteristics. However, the current analysis is sufficient for the purposes of showing that tolerable levels of disequilibrium are associated with at least two of the cases tested, and therefore we are able to draw conclusions from the quasi-equilibrium results with reasonable confidence.

4.5.2 Coastal boundary head correction

The results presented in Sections 4.1 and 4.3 show that water level trends may not necessarily provide an accurate depiction of coastal aquifer status. Werner et al. (2011) advocate comparison of water levels relative to the ocean hydraulic head (i.e., the head at the shoreline for unconfined aquifers), to infer aquifer conditions for the purposes of management decision-making. However, the choice of ocean-head value for rapid comparison to aquifer water levels is not clear. The coastal hydraulic head should account for ocean density effects (Post et al., 2007). For a freshwater-only, single-layer representation of an unconfined coastal aquifer (e.g., the conceptualisation for a freshwater-only groundwater model) the choice of a suitable coastal head can be assessed by simple extension of the theoretical framework presented in Section 4.2.1, at least for idealised conditions. Here, we define an ocean-representative coastal head value (i.e., an equivalent freshwater head) as one that produces a seaward discharge equal to that obtained using the Strack approach for interface flow (i.e., equations (46) to (48)).

Ocean-representative coastal heads in freshwater-only models were obtained for the base cases listed in Table 9, such that the resulting values of q_0 were consistent with q_0 values calculated for interface flow, using the theory in Section 4.2.1. Freshwater-only coastal heads corresponded to density-corrected heads at about halfway through the column of seawater at the shoreline, i.e., $h = \frac{z_0}{2}(1 + \frac{\rho_s}{\rho_f})$, where h is head relative to the base of the aquifer. Using this equation for freshwater-only coastal heads produced q_0 values that deviated from interface flow values by up to 0.3%. The linear nature of the

head-depth relationship in a hydrostatic saltwater column leads to a head correction that is essentially an average of the density-corrected heads at the shoreline. Neglecting the density correction to coastal heads in freshwater-only models caused overestimates in q_0 by up to 50% for the base cases.

4.6 Conclusions

Our review of the literature finds that SWI-induced interface movements and associated changes in seawater volume are neglected in coastal aquifer management studies. Guidance is lacking on the conditions under which this simplified approach may result in erroneous estimates of freshwater volumes and flawed interpretations of water level trend analyses. To address this gap, new equations for freshwater volume in coastal and non-coastal (i.e., freshwater only) aquifers were developed using steady-state, analytic modelling approaches. Homogeneous, isotropic, constant-recharge conditions, and a sharp freshwater-seawater interface, were assumed. Idealised relationships between seawater volume, freshwater volume and water levels, under quasi-equilibrium conditions (i.e., assuming steady-state conditions prevail during transient scenarios), were generated using the new equations. Examination of the quasi-equilibrium approximation demonstrated that two of the three base cases (comprising published parameter sets from case studies) had only minor disequilibrium. A sensitivity analysis indicated that the quasi-equilibrium assumption can be a reasonable approximation for shallow aquifers with high hydraulic conductivity and low effective porosity.

The results of the steady-state analyses demonstrate that seawater volume changes can impact significantly on coastal aquifer water level trends, in comparison to non-coastal

aquifers under otherwise similar conditions. Further, it was found that as freshwater volume is reduced (e.g., due to extraction or declining recharge), seawater volumes impose stronger controls on water level decline, whereby the watertable becomes increasingly unresponsive to changes in freshwater volume. For example, $\Delta V_{sw}/\Delta V_f$ changes from -0.10 to -0.75 (in two of the three base cases) with a 15% reduction in V_f. This indicates that at least 75% of further freshwater volume reductions were replaced by seawater in these cases and, as such, water levels were relatively unresponsive under these conditions. A significant difference in rates of water level decline in coastal and non-coastal aquifers was obtained for reductions in V_f. Water levels are relatively insensitive to freshwater storage change in situations involving a high mixed convection ratio. The sensitivity analysis showed that water level trends are most affected by SWI (i.e., caused by declining freshwater volume) in deep unconfined aquifers with high hydraulic conductivity, low net recharge and small inland extent.

Seawater volume changes (over an assumed timescale) were found to be a significant component of the water balance (i.e., between 10% and 31% when compared to freshwater discharge to the sea), for the three base cases. In addition, coastal aquifer water balances were found to be most sensitive to changes in seawater volume within deep aquifers characterised by low hydraulic conductivity and low freshwater discharge.

In view of the short-comings associated with the use of temporal water level trends to assess coastal aquifer status, the comparison of groundwater levels relative to the hydraulic head imposed by the ocean, accounting for density effects, is recommended. A representative head for the coastal boundary in freshwater-only representations of

unconfined aquifers is proposed that produces reasonable fluxes of freshwater discharge to the sea. This new equation for coastal head adds to the Post et al. (2007) discussion of freshwater head calculations. It provides a first-order estimate of the value that near-shoreline watertable levels should exceed to maintain a discharge to the sea and to avoid SWI issues.

This paper offers insight into the potential influence and significance of SWI-induced changes in seawater volumes within coastal aquifers. For the base cases, changes in seawater volume need to be considered when using water level trends as a measure of sustainability (e.g., within trigger-level management approaches). The method presented here can be rapidly applied to assess the need to consider seawater volumes within specific cases. It has also been shown (for the base cases) that changes in seawater volume need to be included within water balance assessments. Failure to account for changes in seawater volume within coastal aquifers may result in the over-estimation of freshwater volume, potentially leading to the over-allocation of water from these aquifers.

Chapter 5

An assessment of seawater intrusion overshoot using physical and numerical modelling

Abstract

In recent years, a number of numerical modelling studies of transient sea-level rise (SLR) and seawater intrusion (SWI) in flux-controlled systems have reported an overshoot phenomenon, whereby the freshwater-saltwater interface temporarily extends further inland than the eventual steady-state position. In this study, we have carried out physical sand tank modelling of SLR-SWI in a flux-controlled unconfined aquifer setting to test if SWI overshoot is a measurable physical process. Photographs of the physical SLR experiments show, for the first time, that an overshoot occurs under controlled laboratory conditions. A sea-level drop (SLD) experiment was also carried out, and overshoot was again observed, whereby the interface was temporarily closer to the coast than the eventual steady-state position. This shows that an overshoot can occur for the case of a retreating interface. Numerical modelling corroborated the physical SLR and SLD experiments. The magnitude of the overshoot for SLR and SLD in the physical experiments was 24% of the change in steady-state interface position, albeit

---

This Chapter is based on the following publication: Morgan LK, Stoeckl L, Werner AD, Post VEA, 2013. Assessment of seawater intrusion overshoot using physical and numerical modelling, Water Resources Research 49, 6522-6526. doi:10.1002/wrcr.20526.

the laboratory setting is designed to maximise overshoot extent by adopting high groundwater flow gradients and large and rapid sea-level changes. While the likelihood of overshoot at the field scale appears to be low, this work has shown that it can be observed under controlled laboratory conditions.

5.1 Introduction

Changes in the hydrology of the coastal zone can cause landward movement of seawater, a process referred to as seawater intrusion (SWI). Recently, the impact of sea-level rise (SLR) on SWI has received considerable attention. SLR and SWI have been assessed using steady-state sharp interface analytic modelling by Werner and Simmons (2009) and Werner et al. (2012). They found the inland boundary condition to be important in determining SLR-induced SWI, with greatest change occurring for head-controlled conditions, compared to flux-controlled conditions. Transient numerical modelling of SLR and SWI by Watson et al. (2010) encountered an overshoot in SWI. That is, the freshwater-saltwater interface moved temporarily inland beyond the final steady-state position. Chang et al. (2011) also observed an overshoot in SWI; however, they needed to use unrealistically high specific storage values to simulate the overshoot phenomenon within field-scale settings.

A flux-controlled inland boundary condition was applied by Watson et al. (2010) and Chang et al. (2011), whereby the change in hydraulic head at the coast (due to SLR) is followed by a rise of the water table throughout the domain, meaning that the pre-SLR seaward flux of fresh groundwater is eventually restored. Watson et al. (2010) and

Chang et al. (2011) linked the overshoot to this rise in the water table and the time it takes to occur, with overshoot being largest in systems where water table rise is slowest.

While SWI overshoot has been observed for a selection of cases involving numerical simulations of transient SLR-SWI, it has not been confirmed by physical measurements. We address this gap using physical sand tank modelling of SLR-SWI.

The objective of this work is to test whether SWI overshoot is a physical phenomenon that is reproducible under controlled laboratory conditions. Given this objective, laboratory conditions were designed to be especially conducive to SWI overshoot, based on indications from previous modelling studies (Watson et al., 2010; Chang et al., 2011) regarding the propensity for overshoot to occur. Flux-controlled conditions were employed because the foregoing literature suggests that head-controlled conditions may preclude SWI overshoot. Additionally, the case of a sea-level drop (SLD) was examined to ascertain whether overshoot occurs for the situation of a retreating interface. Overshoot associated with a SLD (i.e., involving the interface retreating further toward the coast than the steady-state position) has not been considered previously, although Goswami and Clement (2007) have considered transport processes associated with intruding and receding SWI under varying hydraulic gradients using sand box experiments. We carried out numerical modelling of both the SLR and SLD physical experiments to provide confidence in the results of the physical experiments and additional diagnostics.

5.2 Experimental methods and materials

5.2.1 Physical model

The apparatus used for the physical modelling was essentially the same as that used by Stoeckl and Houben (2012) in their investigation of flow dynamics in freshwater lenses, except the setup was modified for the situation of SLR in an unconfined aquifer with fixed inland flux (Figure 13). A transparent acrylic box of 2.0 m length, 0.5 m height and 0.05 m width was used. An unconfined aquifer cross section was simulated by placing quartz sand homogeneously into the box, with a sloping beach face (slope of 37 degrees) at the left side of the box. The sand body was 32 cm high and 183 cm in length. The grain size distribution of the medium sand (d_{10} = 0.44 mm and d_{50} = 0.62 mm) was optically determined using a Camsizer® (Retsch Technology, Germany), with a measurement range of 30 µm to 30 mm. A hydraulic conductivity (K) value of 0.0022 m s^{-1} was obtained using the grain size distribution and Hazen's equation [*Fetter*, 2001]. In addition, a mean K of 0.0015 m s^{-1} (± 0.0001 m s^{-1}) was obtained using Darcy constant-head conductivity tests. Porosity n_e [-] was calculated based on densities determined using a helium pycnometer (Micromeritics®, Germany) and found to be 0.45. Water densities were obtained using a DMA 38 density meter (Anton Paar, Austria). Freshwater density was determined to be 996.9 kg m^{-3} at 25 °C. Freshwater was coloured yellow using uranine. Saltwater, with a density of 1015.1 kg m^{-3}, was coloured red using eosine. Both uranine and eosine tracer concentrations were 0.3 g L^{-1}.

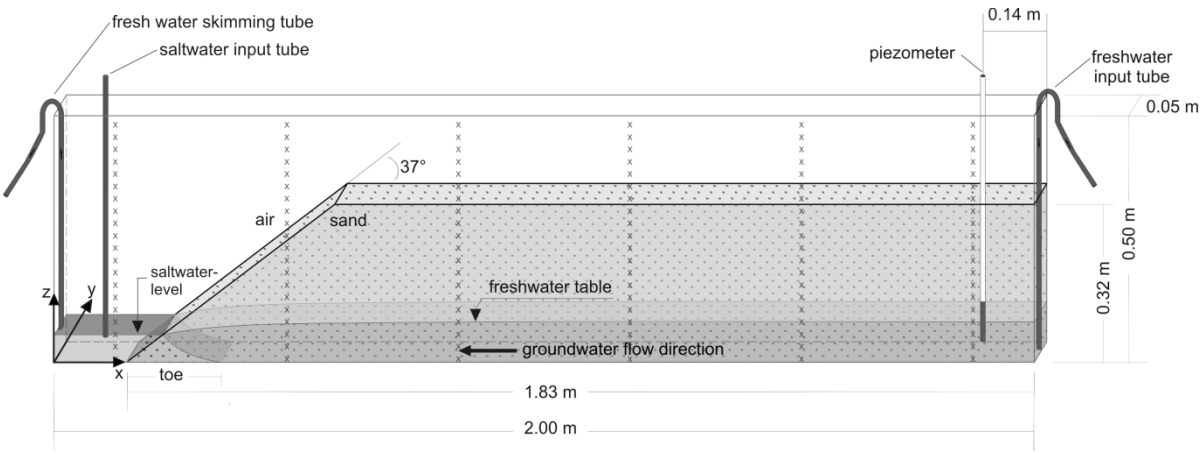

Figure 13. Schematic diagram of the physical model.

A fixed-flux inland boundary condition was imposed using 4 tubes attached to a peristaltic pump. The tube outlets were at the right-hand edge of the sand box, and were equally spaced in the vertical direction below the water table. The flow was distributed equally between the tubes, with a total flux of 5.7 x 10^{-3} m^3 d^{-1}. This gave rise to a head of 3.8 cm at the inland boundary, with the bottom of the sand tank used as the datum. A small saturated thickness was used in the physical experiments in order to achieve a relatively large aquifer length to thickness ratio. Watson et al. (2010) found (numerically) that a large aspect ratio was more likely to produce an overshoot. A constant water level was maintained in the saltwater reservoir at the left side of the sand box, simulating the sea. Freshwater discharge from the aquifer into the ocean formed a thin layer in the saltwater reservoir, and this was removed using skimming tubes, fixed in position. The saltwater reservoir was supplied continuously with additional saltwater to maintain the water level and avoid dilution.

Initially, constant boundary conditions were maintained for 12 h to achieve a steady-state interface. Steady-state conditions were confirmed by monitoring the interface position for a one-hour period, over which time it remained stationary. The interface

was visually approximated as the mid-point of the transition zone between saltwater and freshwater in the aquifer. SLR was simulated by augmenting the inflow rate of saltwater for a period of 6 min, raising the sea level from 2.4 cm to 4.8 cm. A slow rate of SLR was implemented so as not to disturb the stability of the sloping beach face. Photographs showing the interface location, wedge toe position and piezometric head at the inland boundary were taken every 3 min for the first 2 h, and every 15 min for the following hour, using a Canon Ixus 220 HS camera. The wedge toe position (the intersection of the interface with the base of the aquifer) was marked along the base of the sand tank at regular time intervals during the experiment and measured using a scale along the horizontal base of the sand box, with the left-hand edge of the sand tank as the datum. The piezometric head was measured from the photographs using a scale adjacent to the piezometer, with the aquifer base as the datum.

A SLD experiment was performed using the same general sand tank configuration as described above. After 12 h of equilibrium at a sea level of 4.6 cm, the sea level was dropped from 4.6 cm to 2.4 cm. This was achieved by readjusting the skimming tubes to a height of 2.4 cm above the model base and increasing the pumping rate over a time period of approximately 3 min.

5.2.2 Numerical model

The physical SLR and SLD experiments were simulated using the finite-element code FEFLOW 6.0, which considers variably saturated, density-dependent flow and solute transport processes (Diersch, 2005). The numerical model was assumed to be a unit-width aquifer (2D) and hence the flux at the inland boundary Q_0 was scaled to 0.114 m^3

d^{-1}. The coast was simulated using Dirichlet boundary conditions for head and concentration. A constraint was applied to the Dirichlet-type concentration boundary such that seawater concentration (C = 1) occurred only at inflow sections. The concentration of inflows through the inland boundary was C = 0 (representing freshwater). Inflows at the inland boundary were applied using a Neumann boundary condition for flux. A seepage face was expected to occur in the physical model and was implemented in the numerical model using a seepage face boundary condition along the sloping beach face, whereby the model determined the exit face for discharging groundwater. The seepage face boundary was realised by the application of a fixed head boundary (with head equal to the elevation of each node) that is only active if there is flow out of the model. Otherwise, the sloping beach face was a no-flow boundary above the seepage face.

A trapezoidal mesh with 19,737 elements and 10,118 nodes was used. The grid was refined in the region close to the ocean (i.e., where the interface is located) to avoid numerical dispersion and oscillation, and to increase the accuracy of simulating sharp concentration gradients. Grid discretisation in this region was $\Delta x \approx 2$ mm and $\Delta z \approx$ 2mm. Automatic time-stepping was used with an upper step size limit of 0.0002 d. The unsaturated zone was modelled using van Genuchten (1980) functions, with a curve fitting parameter (α) of 30 m^{-1} and a pore size distribution index (n) of 3. These parameters are similar to those adopted by Jakovovic et al. (2011), who also used medium sand. A K of 0.0015 ms^{-1}, n_e [-] of 0.45 and density ratio δ [-] of 0.018 were applied, according with physical modelling values. δ is defined as $\delta = (\rho_s - \rho_f)/\rho_f$, where ρ_f and ρ_s are freshwater and saltwater densities [ML^{-3}], respectively. Longitudinal

and transverse dispersivities were set to 5 x 10^{-3} m and 5 x 10^{-4} m, respectively. The molecular diffusion coefficient was set to 10^{-9} m^2s^{-1}.

Following the establishment of steady-state conditions, an instantaneous change in sea level was applied in the SLR and SLD numerical models. This is a simplification of the physical experiments, where the same sea level changes were considered, but were not instantaneous. This simplification is expected to result in a shorter time to maximum and minimum SWI extent for SLR and SLD, respectively. However, the effect is not expected to be large given that the rates of SLR and SLD in the physical experiments are reasonably rapid. The wedge toe was defined as the point of intersection of the 50% seawater isochlor with the aquifer basement.

5.3. Results and Discussion

5.1 Physical model

The approximate interface location was traced on the front glass of the sand tank after 0, 9, 21 and 120 min (Figure 14). After SLR, the shape of the interface was temporarily more concave than at steady-state (Figure 14b). The degree of concavity reduced after about 21 min (Figure 14c). There was a reduction in interface sharpness for about 45 min following SLR, as expected given the increased dispersion for moving interfaces observed by Werner et al. (2009). A seepage face was evident, whereby freshwater discharged through the face of the sloping beach face above sea level.

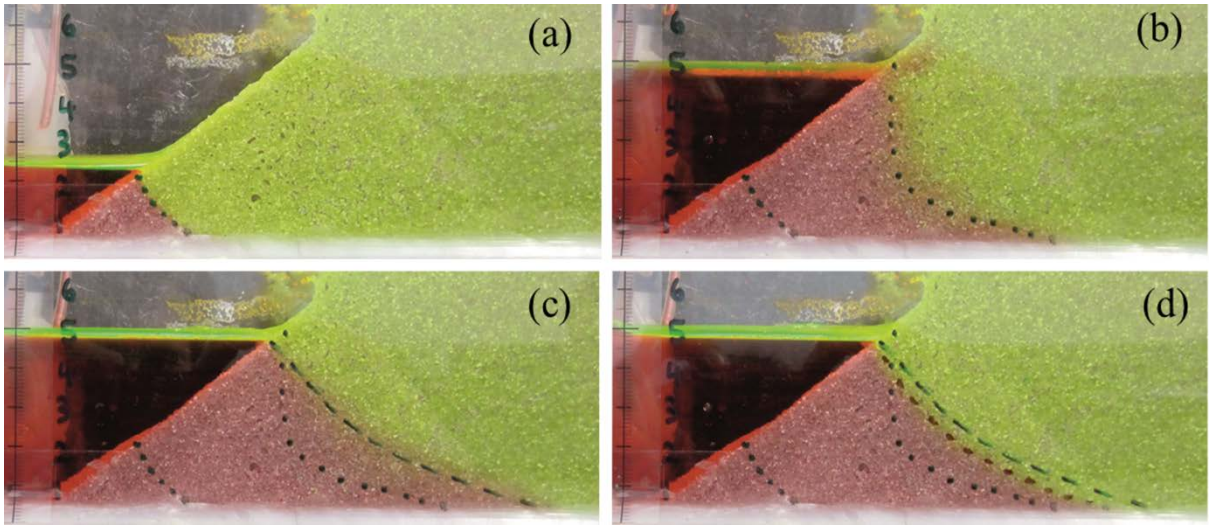

Figure 14. Images from the SLR physical experiment: (a) 0 min, (b) 9 min, (c) 21 min, (d) 2 h. The portion of the sand tank shown above is from x = 17 to 35 cm (where x = 0 cm is at the left-hand edge of the sand tank) and from z = 0 to 6.5 cm.

As shown in Figure 14, an overshoot was observed within the physical experiment. The interface moved inland following the commencement of SLR and reached a maximum inland extent of 33 cm (i.e., toe position) after around 30 min (Figure 15). The movement of the interface then reversed and moved back by 2 cm toward the coast, to the eventual steady-state position of 31 cm (after 120 min). The SWI overshoot in this experiment was therefore 2 cm, or 24% of the change in steady-state toe position (the steady-state pre-SLR toe position was 22.5 cm). The water level in the piezometer at the inland boundary rose 2.1 cm (from 3.8 cm to 5.9 cm) in response to the 2.4 cm rise in sea level (Figure 15). The water level in the piezometer had re-equilibrated after about 30 min. Water level rise at the inland boundary was less than SLR, as expected, because the relationship between flux and head difference in an unconfined coastal aquifer is non-linear (Strack, 1976).

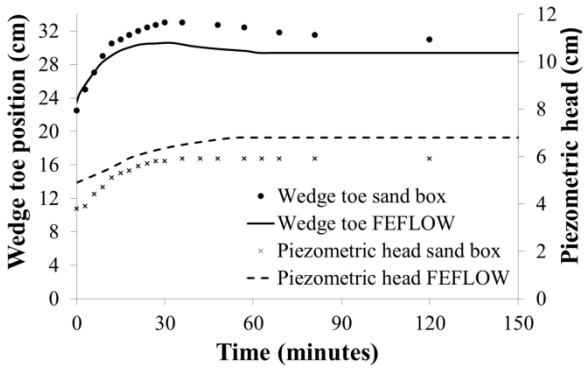

Figure 15. Wedge toe position and piezometric head (at the inland boundary) for the SLR physical modelling experiment and FEFLOW numerical simulation.

An overshoot was also observed in the SLD experiment (see Figure 16). The steady-state toe position was 29.4 cm prior to SLD. The wedge toe reached a minimum value of 21 cm after 12 min and then increased to a steady-state value of 22.6 cm after 75 min. A 1.6 cm overshoot was therefore observed. The SLD overshoot is commensurate with the SLR overshoot; i.e., both being 24% of the change in steady-state wedge toe location. The water level in the piezometer at the inland boundary dropped 1.9 cm (from 6.0 cm to 4.1 cm) in response to the 2.2 cm SLD (Figure 16). As with the SLR experiment, the water level at the inland boundary re-equilibrated after around 30 min.

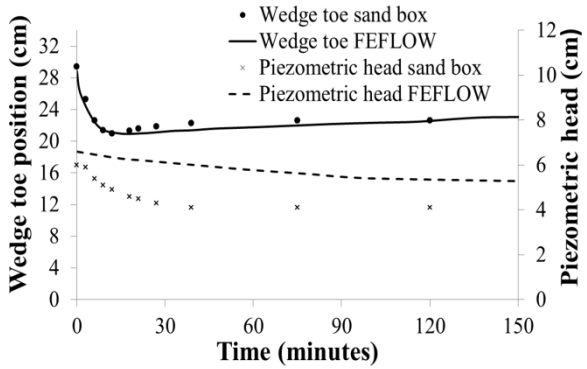

Figure 16. Wedge toe position and piezometric head (at the inland boundary) for the SLD physical modelling experiment and FEFLOW numerical simulations.

5.3.2 Numerical model

Transient wedge toe positions obtained from the numerical model were compared to the results of the physical experiments and a reasonable match was obtained (Figures 15 and 16). An overshoot of 1.2 cm was simulated in the SLR numerical model, which was 20% of the change in steady-state wedge toe position. A 2.4 cm overshoot was simulated in the SLD numerical model, representing 43% of the change in steady-state wedge toe position. Time to maximum SWI extent for the SLR simulation (32 min) and time to minimum SWI extent for the SLD simulation (14 min) were similar to results from the physical experiments.

The numerical modelling results show that time to maximum SWI extent for an instantaneous SLR is longer than time to minimum SWI extent for an instantaneous SLD. Temporal asymmetry of the overshoot was expected, given that Watson et al. (2010) previously found response times under SLR to be greater than SLD for instantaneous changes in sea level (although only for a single pair of SLR and SLD simulations). Also, Chang and Clement (2012) have reported temporal asymmetry for intrusion and recession processes under changes of flux at the inland boundary, with intrusion taking longer than recession.

Additional numerical modelling was carried out to explore the influence of the unsaturated zone on the overshoot in the SLR physical experiment. This was achieved through varying the van Genuchten (1980) curve fitting parameter, α. A larger value of α (i.e., 50 m^{-1}, which applies to medium sand (Jakovovic et al., 2011)) reduced the capillary fringe thickness and increased the overshoot (from 1.2 cm to 1.7 cm). A

smaller value of α (i.e., 10 m^{-1}, which applies to a sandy loam (Carsel and Parish, 1988)) increased the capillary fringe and resulted in negligible overshoot. Changes in overshoot extent with α are attributed to changes in the capillary fringe thickness, which in the case of α equal to 10 m^{-1} effectively doubled the saturated thickness, thereby reducing the aspect ratio by approximately 50%. The lower aspect ratio produced a smaller overshoot, in agreement with the numerical simulations of Watson et al. (2010). Numerical modelling was also used to explore the influence of the sloping beach face on the overshoot in the SLR physical experiment. An overshoot of 1 cm was simulated using a vertical beach face, indicating that the sloping beach face does not control the extent of overshoot, as expected given that overshoot in previous numerical modelling studies (Watson et al., 2010; Chang et al., 2011) occurred with vertical coastal boundaries.

Although the cause of SWI overshoot has not been systematically explored within this study, the numerical modelling results indicate that overshoot is associated with a time lag in the response of the flow field following SLR. Velocity vectors showed that reversal of the wedge toe movement occurs as freshwater outflow at the coast approaches equilibrium. It follows that overshoot will be larger in systems where it takes longer for freshwater outflow to re-equilibrate. This agrees with the previous results of Watson et al. (2010) and Chang et al. (2011).

5.4. Conclusions

Physical sand tank experiments have been undertaken to assess SWI overshoot observed previously in numerical modelling studies of SLR-SWI by Watson et al.

(2010) and Chang et al. (2011). An overshoot was observed in the SLR physical experiment and images of the overshoot are presented. A SLD experiment was also carried out and the overshoot was again observed. These are the first documented cases of overshoot in a laboratory setting, and the first time overshoot for a retreating interface has been reported.

The transient wedge toe position obtained from the physical experiments was compared to numerical modelling results, and a reasonable match was obtained, with an overshoot simulated numerically for both the SLR and SLD cases. This provides confidence in the results of the physical experiments.

The magnitude of the overshoot was 24% of the change in steady-state wedge toe for both SLR and SLD physical experiments. As such, SWI overshoot was found to be relatively large, albeit the laboratory setting is designed to maximise overshoot extent by adopting high groundwater flow gradients and large and rapid sea-level changes. Using field-scale simulation results, Chang et al. (2011) concluded that it is difficult to observe overshoot in realistic aquifers. Hence, it is unlikely that overshoot would be a concern in real field-scale problems. Nevertheless, we demonstrate that overshoot is physically plausible, and can be produced in controlled laboratory experiments.

Acknowledgements

Thanks to Georg Houben for the helpful comments. The support of Jan Bockholt for the experimental work is gratefully acknowledged as well as Ulrich Gersdorf for his help with the elaboration of Figure 13. Thanks also to Mothei Lenkopane for helpful

discussions on the seepage face boundary condition in FEFLOW. We also wish to thank Prabhakar Clement, Christian Langevin and three anonymous reviewers whose helpful suggestions have improved this work. This work was part funded by the National Centre for Groundwater Research and Training, a collaborative initiative of the Australian Research Council and the National Water Commission.

Chapter 6

Conclusions

SWI is a complex process that involves variable-density flow, solute transport and hydrochemical processes, which can make SWI assessment relatively difficult and expensive. The aim of this thesis is the development, application and critical assessment of practical (i.e., rapid, inexpensive) analytic modelling approaches for investigating and assisting in the management of SWI. This Chapter summarises the main conclusions.

The assessment of SWI vulnerability over large scales has generally been carried out using mainly qualitative methods, which consider only a subset of the factors thought to impact SWI. Recently, an alternative to the above-mentioned large-scale methods has been developed by Werner et al. (2012). The method is based on the steady-state, sharp-interface equations of Strack (1976), and therefore incorporates the physical mechanics of SWI, albeit under highly idealised conditions. In Chapter 2, the Werner et al. (2012) method was applied to the multilayered Willunga Basin, South Australia to explore SWI vulnerability arising from extraction, recharge change and sea-level rise (SLR). The study provides insight into the relative vulnerability of aquifers at the site and has assisted with the determination of research priorities as part of an on-going field-based investigation. Limitations of the vulnerability indicators method, associated with the

sharp-interface and steady-state assumptions, were addressed using numerical modelling to explore transient, dispersive SWI caused by SLR.

Freshwater lenses on small islands are some of the most vulnerable aquifer systems in the world. However, there is currently little guidance on methods for rapidly assessing the vulnerability of freshwater lenses to the potential effects of climate change. In Chapter 3, SWI vulnerability indicator equations have been developed that describe the propensity for change in SWI extent for freshwater lenses in strip islands under climate change-induced SLR and recharge change. The influence of LSI under SLR was included in these equations. This work extends that of Werner et al. (2012), who developed SWI vulnerability indicators for unconfined and confined aquifer systems and did not consider LSI. Several inferences regarding SWI vulnerability in freshwater lenses can be made from the analysis: (1) SWI vulnerability indicators for SLR (under flux-controlled conditions) are proportional to lens thickness (or volume) and the rate of LSI and inversely proportional to island width; (2) SWI vulnerability indicators for recharge change (under flux-controlled conditions) are proportional to lens thickness (or volume) and inversely proportional to recharge; (3) SLR has greater impact under head-controlled conditions rather than flux-controlled conditions, whereas the opposite is the case for LSI and recharge change. The equations were applied to three case studies to produce a ranking based on vulnerability to SLR and recharge change. Logarithmic sensitivities were used to explore the relative contributions of SLR, LSI and recharge change to SWI vulnerability. Despite the limitations of the approach that arise from the simplifying assumptions (e.g., steady-state, sharp interface, homogeneous aquifer, no outflow face), we suggest that the SWI vulnerabilities presented here provide informative first-pass estimates of the relative threats of climate change (SLR and

recharge change) to the freshwater lens systems of strip islands. Example applications to several case studies illustrate use of the method for rapidly ranking lenses according to vulnerability, thereby allowing for prioritisation of areas where further and more detailed SWI investigations may be required.

The changes in seawater volumes caused by seawater intrusion are often neglected in coastal aquifer management studies. The conditions under which this can result in significant water balance errors are not well understood. Interface movements also influence temporal trends in coastal aquifer water levels, but there is little guidance on this effect. In Chapter 3, steady-state, sharp-interface, analytic modelling was used to generate idealised relationships between seawater volume, freshwater volume and water levels. The approach assumes quasi-equilibrium conditions, which were evaluated using a selection of transient, dispersive simulations. The results demonstrate that seawater volume changes can influence significantly coastal aquifer water level trends, relative to the corresponding non-coastal aquifer situation, particularly within deep aquifers with high hydraulic conductivity and low net recharge. It was also shown that seawater volume changes can be a significant component of coastal aquifer water balances, e.g., relative to freshwater discharge to the sea, especially within deep aquifers characterised by low hydraulic conductivity and low freshwater discharge. Transient simulations show that steady-state conditions are a reasonable approximation for a range of transient seawater intrusion situations, including two of the three cases considered in this analysis. We conclude that changes in seawater volumes should be included routinely in coastal aquifer water balances. Also, temporal trends in coastal aquifer water levels may not provide an adequate measure of freshwater storage trends. It follows that the assessment of coastal aquifer condition should consider groundwater

levels relative to the hydraulic head imposed by the ocean, accounting for density effects.

In recent years, a number of numerical modelling studies of transient SLR and SWI in flux-controlled systems have reported an overshoot phenomenon, whereby the freshwater-saltwater interface temporarily extends further inland than the eventual steady-state position. In Chapter 5, we describe physical sand tank modelling of SLR-SWI in a flux-controlled unconfined aquifer setting, which was carried out to test if SWI overshoot is a measurable physical process. Photographs of the physical SLR experiments show, for the first time, that an overshoot occurs under controlled laboratory conditions. A sea-level drop (SLD) experiment was also carried out, and overshoot was again observed, whereby the interface was temporarily closer to the coast than the eventual steady-state position. This shows that an overshoot can occur for the case of a retreating interface. Numerical modelling corroborated the physical SLR and SLD experiments. The magnitude of the overshoot for SLR and SLD in the physical experiments was 24% of the change in steady-state interface position, albeit the laboratory setting was designed to maximise overshoot extent by adopting high groundwater flow gradients and large and rapid sea-level changes. While the likelihood of overshoot at the field scale appears to be low, this work has shown that it can be observed under controlled laboratory conditions.

References

Ataie-Ashtiani B, Werner AD, Simmons CT, Morgan LK, Lu C, 2013. How important is the impact of land-surface inundation on the impact of sea-level rise on seawater intrusion? Hydrogeology Journal 21(7), 1673-1677. doi: 10.1007/s10040-013-1021-0

Australian Bureau of Statistics (ABS), 2004. Year book of Australia, http://www.abs.gov.au/Ausstats/abs@.nsf/Previousproducts/1301.0Feature%20Article32004 (accessed 10 April 2012).

Bakker M, 2006. Analytic solutions for interface flow in combined confined and semi-confined, coastal aquifers, Advances in Water Resources 29: 417–425.

Barlow PM, Reichard EG, 2010. Saltwater intrusion in coastal regions of North America, Hydrogeology Journal 18(1), 247-260.

Bear J, 1972. Dynamics of fluids in porous media, Dover publications.

Bekesi G, McGuire M, Moiler D, 2009. Groundwater allocation using a groundwater level response management method-Gnangara groundwater system, Western Australia. Water Resources Management 23, 1665-1683.

Bocanegra E, Da Silva Jr GD, Custodio E, Manzano M, Montenegro S, 2010. State of knowledge of coastal aquifer management in South America, Hydrogeology Journal 18(1), 261-267.

Bredehoeft JD, 2002. The water budget myth revisited: Why hydrogeologists model, Ground Water 40, 340-345.

Brown K, Harrington G, Lawson J, 2006. Review of groundwater resource condition and management principles for the Tertiary Limestone Aquifer in the South East of South Australia, Department of Water, Land and Biodiversity Conservation, Report DWLBC 2006/2, Government of South Australia, Adelaide, www.waterconnect.sa.gov.au/BusinessUnits/InformationUnit/Technical%20Publications/dwlbc_report_2006_02.pdf (accessed December 5, 2011).

Carsel RF, Parrish RS, 1988. Developing joint probability distributions of soil water retention characteristics, Water Resources Research, 24(5), doi: 10.1029/WR024i005p00755.

Chachadi AG, Lobo-Ferreira JP, 2007. Assessing aquifer vulnerability to seawater intrusion using GALDIT method: Part 2 - GALDIT Indicators Description, Water in Celtic Countries: Quantity, Quality and Climate Variability, 310, 172-180.

Chang SW, Clement TP, 2012. Experimental and numerical investigation of saltwater intrusion dynamics in flux controlled groundwater systems, Water Resources Research 48(9), doi:10.1029/2012WR012134.

Chang SW, Clement TP, Simpson MJ, Lee KK, 2011. Does sea-level rise have an impact on saltwater intrusion? Advances in Water Resources 34(10), 1283-1291, doi:10.1016/j.advwatres.2011.06.006.

Cheng AHD, Benhachmi MK, Halhal D, Ouazar D, Naji A, Harrouni KE, 2004. Pumping optimization in saltwater-intruded aquifers, in Cheng AHD, Ouazar D (Eds.), Coastal aquifer management: Monitoring, modeling and case studies, CRC Press, 178-197.

Cheng AHD, Ouazar D, 1999. Analytical solutions, in Bear J, Cheng AHD, Sorek S, Ouazar D, Herrera I (Eds.), Seawater intrusion in coastal aquifers – concepts, methods and practices. Kluwer Academic Publishers, Dordrecht, The Netherlands.

Chui TFM, Terry JP, 2013. Influence of sea-level rise on freshwater lenses of different atoll island sizes and lens resilience to storm-induced salinization, Journal of Hydrology 502, 18-26, http://dx.doi.org/10.1016/j.jhydrol.2013.08.013.

Church JA, White NJ, Hunter JR, 2006. Sea-level rise at tropical Pacific and Indian Ocean islands, Global and Planetary Change 53, 155-168, doi: 10.1016/j.gloplacha.2006.04.001.

Cooper JHH, 1964. A hypothesis concerning the dynamic balance of fresh water and salt water in a coastal aquifer, U.S. Geological Survey Water Supply Paper, 1613-C.

Custodio E, 1987. Prediction methods, Chapter 8, in Bruggerman GA, Custodio E (Eds.) Studies and reports in hydrology, no. 45, Groundwater problems in coastal areas, UNESCO, Paris.

Custodio E, 2002. Aquifer overexploitation: what does it mean? Hydrogeology Journal 10, 254-277, doi:10.1007/s10040-002-0188-6.

Davidson WA, Yu X, 2006. Perth regional aquifer modelling system (PRAMS) model development: Hydrogeology and groundwater modelling, Western Australia Department of Water, Hydrogeological record series HG 20. Government of Western Australia, Perth. www.water.wa.gov.au/PublicationStore/first/71802.pdf (accessed December 10, 2011).

Diersch HJG, 2005. FEFLOW: Finite Element Subsurface Flow and Transport Simulation System, WASY GmbH Institute for Water Resources Planning and Systems Research, Berlin, Germany.

Diersch HJG, Kolditz O, 2002. Variable-density flow and transport in porous media: approaches and challenges, Advances in Water Research 25, 899-944.

FAO, 1997. Seawater intrusion in coastal aquifers: Guidelines for study, monitoring and control, FAO Water Reports no. 11, Food and Agriculture Organization (FAO) of the United Nations, Rome, Italy.

Fetter CW, 1972. Position of the saline water interface beneath oceanic islands, Water Resources Research 8(5), 1307-1315.

Fetter CW, 2001. Applied hydrogeology, 4th ed., Prentice Hall, New Jersey.

Ghassemi F, Molson JW, Falkland A, Alam K, 1999. Three-dimensional simulation of the Home Island freshwater lens: preliminary results, Environmental Modelling and Software 14, 181–190.

Ghyben BW, 1888. Nota in verband met de voorgenomen put-boring nabij Amsterdam (Notes on the probable results of the proposed well drilling in Amsterdam), Tijdschrift van het Koninklijk Institunt van Ingeniers, The Hague, 8-22.

Goswami RR, Clement TP, 2007. Laboratory-scale investigation of saltwater intrusion dynamics, Water Resources Research 43, WO4418, doi: 10.1029/2006WR005151.

Guo W, Langevin C, 2002. User's guide to SEAWAT: A computer program for the simulation of three-dimensional variable-density ground-water flow, USGS Techniques of Water Resources Investigations, Book 6, Chapter A7.

Herzberg A, 1901. Die Wasserversorgung einiger Nordseeb-ider (The water supply on parts of the North Sea coast in Germany), Journal Gabeleucht ung und Wasserversorg ung 44, 815-819, 824-844.

Herzceg AL, Leaney F, 2002. Groundwater replenishment rates to fractured rock and sedimentary aquifers in the McLaren Vale Prescribed Wells Area, Final report to the Onkaparinga Catchment Water Management Board, CSIRO Land and Water, Technical Report 10/02, March 2002.

Intergovernmental Panel on Climate Change (IPCC) 2007. Climate Change 2007: Working group I: The physical science basis. Projections of future changes in climate, http://ipcc.ch/publications_and_data/ar4/wg1/en/spmsspm-projections-of.html (accessed 29 April 2011).

Ivkovic KM, Marshall SK, Morgan LK, Werner AD, Carey H, Cook S, Sundaram B, Norman R, Wallace L, Caruana L, Dixon-Jain P, Simon D, 2012. A national scale vulnerability assessment of seawater intrusion: summary report, Waterlines Report Series No 85, August 2012, National Water Commission, Canberra, http://archive.nwc.gov.au/library.

Jakovovic D, Werner AD, Simmons CT, 2011. Numerical modelling of saltwater up-coning: Comparison with experimental laboratory observations, Journal of Hydrology 402, 261-273, doi:10.1016/j.jhydrol.2011.03.021.

Kabala ZJ, 2001. Sensitivity analysis of a pumping test on a well with wellbore storage and skin, Advances in Water Resources 24, 19-35.

Kacimov AR, Sherif MM, Perret JS, Al-Mushikhi A, 2009. Control of sea-water intrusion by salt-water pumping: Coast of Oman, Hydrogeology Journal 17, 541-558.

Kerrou J, Renard P, Tarhouni J, 2010. Status of the Korba groundwater resources (Tunisia): observations and three-dimensional modelling of seawater intrusion, Hydrogeology Journal 18, 1173-1190.

Ketabchi H, Mahmoodzadeh D, Atai-Ashtiani B, Werner AD, Simmons CT, 2013. Sea-level rise impact on a fresh groundwater lens in two-layer small islands. Hydrological Processes, In press. doi: 10.1002/hyp.10059

Kooi K, Groen J, 2001. Offshore continuation of coastal groundwater systems; predictions using sharp interface approximations and variable density flow modelling, Journal of Hydrology 246: 19-35.

Langevin CD, Thorne D, Dausman AM, Sukop MC, Guo W, 2008. SEAWAT Version 4: A computer program for simulation of multi-species solute and heat transport, USGS Techniques and Methods, Book 6, Chapter A22.

Larabi A, Faouzi M, Cheng AH, 2008. Assessment of groundwater resources in Rmel Coastal aquifer (Morocco), Twentieth Salt Water Intrusion Meeting, Naples, Florida, USA. www.swim-site.org/ (accessed November 20, 2011).

Lobo-Ferreira JP, Chachadi AG, Diamantino C, Henriques MJ, 2007. Assessing aquifer vulnerability to seawater intrusion using the GALDIT method: part 1 - application to the Portuguese Monte Gordo aquifer, In proceedings, Lobo Ferreira JP, Viera JMP (Eds.), Water in Celtic Countries: Quantity, Quality and Climate Variability, IAHS

Publication 310, International Association of Hydrological Sciences, Wallingford, 161-171.

Mantoglou A, 2003. Pumping management of coastal aquifers using analytical models of saltwater intrusion, Water Resources Research 39(12), doi: 10.1029/2002WR001891.

Mimura N, 1999. Vulnerability of island countries in the South Pacific to sea level rise and climate change, Climate Research 12, 137-143.

Moe H, Hossain R, Fitzgerald R, Banna M, Mushtaha A, Yaqubi A, 2001. Application of 3-Dimensional Coupled Flow and Transport Model in the Gaza Strip, First International Conference on Saltwater Intrusion and Coastal Aquifers – Monitoring, Modeling, and Management, Essaouira, Morocco, April 23-25, 2001.

Morgan LK, Stoeckl L, Werner AD, Post VEA, 2013a. Assessment of seawater intrusion overshoot using physical and numerical modelling, Water Resources Research 49, 6522-6526. doi:10.1002/wrcr.20526.

Morgan LK, Werner AD, 2014. Seawater intrusion vulnerability indicators for freshwater lenses in strip islands, Journal of Hydrology 508, 322-327. doi:10.1016/j.jhydrol.2013.11.002.

Morgan LK, Werner AD, Carey H, 2013b. A national-scale vulnerability assessment of seawater intrusion: Seawater intrusion vulnerability indexing – quantitative, Record

2013/20, Geoscience Australia, Canberra, and National Centre for Groundwater Research and Training, Adelaide, ISBN: 978-1-922201-50-8.

Morgan LK, Werner AD, Ivkovic KM, Carey H, Sundaram B, 2013c. A national-scale vulnerability assessment of seawater intrusion: First-order assessment of seawater intrusion for Australian case study sites, Record 2013/19, Geoscience Australia, Canberra, and National Centre for Groundwater Research and Training, Adelaide, ISBN: 978-1-922201-49-2.

Morgan LK, Werner AD, Morris MJ, Teubner M, 2013d. Application of a rapid-assessment method of SWI: Willunga Basin, South Australia, In Wetzelhuetter C, (Ed.), Groundwater in the Coastal Zones of Asia - Pacific, Coastal Research Library, Vol. 7, Springer.

Morgan LK, Werner AD, Simmons CT, 2012. On the interpretation of coastal aquifer water level trends: A precautionary note, Journal of Hydrology 470-471, 280-288, doi:10.1016/j.jhydrol.2012.09.001.

Oberdorfer JA, Buddemeier RW, 1988. Climate change effects on reef island resources, In proceedings, Choat JH, et al. (Eds.), Sixth International Coral Reef Symposium, 8-12 August 1988, Townsville, Australia, 3, 523-527.

Ozyurt G, 2007. Vulnerability of coastal areas to sea level rise: A case study on Goksu Delta, Masters Thesis, Department of Civil Engineering, Middle East Technical University, Ankara, Turkey.

Pool M, Carrera J, 2011. A correction factor to account for mixing in Ghyben-Herzberg and critical pumping rate approximations of seawater intrusion in coastal aquifers, Water Resources Research, 47, W05506, doi:10.1029/2010WR10256.

Post V, 2005. Fresh and saline groundwater interaction in coastal aquifers: Is our technology ready for the problems ahead? Hydrogeology Journal 13, 120-123.

Post V, Kooi H, Simmons C, 2007. Using hydraulic head measurements in variable-density ground water flow analyses, Ground Water 45(6), 664-671.

Qahman K, Larabi A, 2006. Evaluation and numerical modelling of seawater intrusion in the Gaza aquifer (Palestine), Hydrogeology Journal 14, 713-728.

Rasser PE, 2001. Calibration of numerical models with application to groundwater flow in the Willunga Basin, S.A., Thesis submitted for the degree of Master of Science in Applied Mathematics at Adelaide University, Adelaide, Australia.

Schafer DB, Johnson SL, 2009. Groundwater resource assessment of the Western Busselton-Capel area, Western Australia Department of Water, Report no. HG38, Government of Western Australia, Perth, www.water.wa.gov.au/PublicationStore/first/90034.pdf (accessed October 20, 2011).

Sherif MM, Singh VP, 1999. Effect of climate change on sea water intrusion in coastal aquifers, Hydrological Processes 13(8), 1277–1287.

Singh, VS, Gupta CP, 1999. Groundwater in a coral island, Environmental Geology 37(1–2), 72-77.

Stoeckl L, Houben G, 2012. Flow dynamics and age stratification of freshwater lenses: Experiments and modelling, Journal of Hydrology 458-459, 9-15, doi: 10.1016/j.jhydrol.2012.05.070.

Strack ODL, 1976. Single-potential solution for regional interface problems in coastal aquifers, Water Resources Research 12, 1165-1174.

Strack ODL, 1989. Groundwater mechanics, Prentice Hall, Englewood Cliffs, New Jersey (out of print, currently published by Strack Consulting Inc.).

Sun H, 2005. Construction, calibration and application of the South West Yarragadee Aquifer Model V2.0, Water Corporation, Perth, www.water.wa.gov.au/PublicationStore/first/82078.pdf (accessed December 12, 2011).

Terry JP, Chui TFM, 2012. Evaluating the fate of freshwater lenses on atoll islands after eustatic sea-level rise and cyclone-driven inundation: A modelling approach, Global and Planetary Change 88-89, 76-84, doi: 10.1016/j.gloplacha.2012.03.008.

Vacher HL, 1988. Dupuit-Ghyben-Herzberg analysis of strip island lenses, Geological Society of America Bulletin 100(4), 580-591.

van Dam JC, 1999. Exploitation, restoration and management, In Bear J, Cheng AHD, Sorek S, Ouazar D, Herrera I (Eds.) Seawater intrusion in coastal aquifers – Concepts, methods and practices, Kluwer Academic Publishers, Dordrecht, The Netherlands, 73-125.

van Genuchten MT, 1980. A closed-form equation for predicting the hydraulic conductivity of unsaturated soils, Soil Science Society of America Journal 44, 892-898, doi:10.2136/sssaj1980.03615995004400050002x.

Varma S, 2009. Southern Perth Basin groundwater resource assessment, Western Australia Department of Water, Report no. HG26, Government of Western Australia, Perth, www.water.wa.gov.au/PublicationStore/first/83807.pdf (accessed December 10, 2011).

Voudouris KS, 2006. Groundwater balance and safe yield of the coastal aquifer system in NEastern Korinthia, Greece, Applied Geography 26, 291-311.

Watson TA, Werner AD, Simmons CT, 2010. Transience of seawater intrusion in response to sea-level rise, Water Resources Research 46, W12533, doi:10.1029/2010WR009564.

Webb MD, Howard KWF, 2010. Modeling the transient response of saline intrusion to rising sea-levels, Ground Water 49(4), 560-569.

Werner AD, 2010. A review of seawater intrusion and its management in Australia, Hydrogeology Journal 18, 285-285.

Werner AD, Alcoe DW, Ordens CM, Hutson JL, Ward JD, Simmons CT, 2011. Current practice and future challenges in coastal aquifer management: Flux-based and trigger-level approaches with application to an Australian case study, Water Resources Management 25(7), 1831-1853.

Werner AD, Bakker M, Post VEA, Vandenbohede A, Lu C, Atai-Ashtiani B, Simmons CT, Barry DA, 2013. Seawater intrusion processes, investigation and management: Recent advances and future challenges, Advances in Water Resources 51, 3-26, http://dx.doi.org/10.1016/j.advwatres.2012.03.004.

Werner AD, Gallagher MR, 2006. Characterisation of sea-water intrusion in the Pioneer Valley, Australia using hydrochemistry and three-dimensional numerical modelling, Hydrogeology Journal 14, 1452-1469.

Werner AD, Jakovovic D, Simmons CT, 2009. Experimental observations of saltwater up-coning, Journal of Hydrology 373, 230-241, doi:10.1016/j.jhydrol.2009.05.004.

Werner AD, Simmons CT, 2009. Impact of sea-level rise on seawater intrusion in coastal aquifers, Ground Water 47(2), 197-204, doi: 10.1111/j.1745-6584.2008.00535.x.

Werner AD, Ward JD, Morgan LK, Simmons CT, Robinson NI, Teubner MD, 2012. Vulnerability indicators of seawater intrusion, Ground Water 50(1), 48-58, doi:10.1111/j.1745-6584.2011.00817.x.

White I, Falkland T, 2010. Management of freshwater lenses on small Pacific islands, Hydrogeology Journal 18, 227-246.

White I, Falkland T, Metutera T, Metai E, Overmars M, Perez P, Dray A, 2007. Climatic and human influences on groundwater in low atolls, Vadose Zone Journal 6(3), 1-10.

Woodroffe CD, 2008. Reef island topography and the vulnerability of atolls to sea-level rise, Global and Planetary Change 62, 77-96.

Zheng C, Bennett GD, 2002. Applied contaminant transport modeling, 2nd edition, Wiley Interscience, New York.

Zulfic D, Harrington N, Evans S, 2007. Uley Basin groundwater modelling project, Volume 2: Groundwater flow model, Department of Water, Land and Biodiversity Conservation, DWLBC Report 2007/04, Government of South Australia, Adelaide, https://www.waterconnect.sa.gov.au/BusinessUnits/InformationUnit/Technical%20Publications/ki_dwlbc_report_2007_04.pdf (accessed December 10, 2011).